MOLECULAR AND CELLULAR BIOLOGY, Sept. 2009, p. 4812–4830 Vol. 29, No. 17
0270-7306/09/$08.00+0 doi:10.1128/MCB.00352-09


# The Alternative TrkAIII Splice Variant Targets the Centrosome and Promotes Genetic Instability▽

Antonietta Rosella Farina,[1]† Antonella Tacconelli,[1]† Lucia Cappabianca,[1] Gesilia Cea,[1] Sonia Panella,[1] Antonella Chioda,[1] Alessandra Romanelli,[2] Carlo Pedone,[2] Alberto Gulino,[3] and Andrew Reay Mackay[1]*

*Department of Experimental Medicine, University of L'Aquila, Via Vetoio, Coppito 2, 67100 L'Aquila, Italy[1]; Department of Biological Science, University of Naples Federico II, Naples, Italy[2]; and Department of Experimental Medicine, University of Rome La Sapienza, Rome, and Neuromed Institute, 86077 Pozzilli, Italy[3]*

Received 18 March 2009/Returned for modification 9 April 2009/Accepted 21 June 2009

**The hypoxia-regulated alternative TrkAIII splice variant expressed by human neuroblastomas exhibits oncogenic potential, driven by in-frame exon 6 and 7 alternative splicing, leading to omission of the receptor extracellular immunoglobulin $C_1$ domain and several N-glycosylation sites. Here, we show that the TrkAIII oncogene promotes genetic instability by interacting with and exhibiting catalytic activity at the centrosome. This function depends upon intracellular TrkAIII accumulation and spontaneous interphase-restricted activation, in cytoplasmic tyrosine kinase (tk) domain orientation, predominantly within structures that closely associate with the fully assembled endoplasmic reticulum intermediate compartment and Golgi network. This facilitates TrkAIII tk-mediated binding of γ-tubulin, which is regulated by endogenous protein tyrosine phosphatases and geldanamycin-sensitive interaction with Hsp90, paving the way for TrkAIII recruitment to the centrosome. At the centrosome, TrkAIII differentially phosphorylates several centrosome-associated components, increases centrosome interaction with polo kinase 4, and decreases centrosome interaction with separase, the net results of which are centrosome amplification and increased genetic instability. The data characterize TrkAIII as a novel internal membrane-associated centrosome kinase, unveiling an important alternative mechanism to "classical" cell surface oncogenic receptor tk signaling through which stress-regulated alternative TrkAIII splicing influences the oncogenic process.**

Alternative splicing is fundamental for differential protein expression from the same gene and not only increases the proteomic complexity of higher organisms (29) but is also involved in cancer pathogenesis, activating several oncogenes and inactivating several oncosuppressors (17).

The neurotrophin receptor tropomyosin-related kinase A (TrkA) is among the proto-oncogenes activated by alternative splicing, with a novel hypoxia-regulated oncogenic alternative TrkAIII splice variant recently identified in advanced-stage human neuroblastomas (NB) and primary glioblastomas (44, 45). In contrast to wild-type TrkAI/TrkAII, the expression of which is associated with better prognosis for NB, induces NB cell differentiation, exhibits a tumor suppressor function in NB models in vivo (9, 19, 22, 30, 44, 45), and may regulate both spontaneous and therapy-induced NB regression (30), TrkAIII is expressed by more-advanced-stage NB and exhibits oncogenic activity in NB models (44, 45). This has challenged the hypothesis of an exclusively tumor-suppressing function for TrkA in NB by providing a way through which tumor-suppressing signals from TrkA can be converted to oncogenic signals from TrkAIII during tumor progression.

The oncogenic potential of TrkAIII, characterized by NIH 3T3 cell transforming and NB xenograft primary and metastatic tumor-promoting activity (44, 45), is driven by in-frame alternative splicing of exons 6 and 7. This results in the omission of the receptor extracellular immunoglobulin $C_1$ (Ig $C_1$) Ig-like domain and several N-glycosylation sites important in regulating TrkA cell surface expression and preventing ligand-independent activation (2, 44, 45, 48). As a consequence, and unlike TrkAI and TrkAII, TrkAIII is not expressed at the cell surface but accumulates in the intracellular membrane compartment, within which it exhibits spontaneous tyrosine kinase (tk) and phosphoinositol-3 kinase (PI3K) activity and induces chronic signaling through PI3K/Akt/NF-κB but not Ras/mitogen-activated protein kinase (MAPK), inducing a more stress-resistant, angiogenic, and tumorigenic NB cell phenotype (44, 45). This differs from ligand-activated cell surface TrkA, which signals transiently through Ras/MAPK in NB cells to induce differentiation and a less angiogenic and tumorigenic NB cell phenotype (9, 19, 22, 30, 44, 45). This difference in signaling provides a potential basis for the opposing tumor-suppressing and oncogenic effects of alternative TrkA splice variants, which may not only depend upon the dislocation of TrkAIII from cell surface caveolae, which are the sites of TrkAI expression and Ras/MAPK signal initiation (45, 48), but also TrkAIII-associated PI3K activity below the Ras/MAPK activation threshold and/or TrkAIII-associated PI3K antagonism of Raf/MEK/extracellular signal-regulated kinase signaling (44). Signal transduction from intracellular TrkAIII bears close resemblance to the transient signaling through PI3K/Akt/NF-κB but not Ras/MAPK induced by A2a adenosine receptor/c-Src-mediated transactivation of immature TrkAI within the Golgi network

* Corresponding author. Mailing address: Section of Molecular Pathology, Department of Experimental Medicine, University of L'Aquila, Coppito 2, Via Vetoio, L'Aquila 67100, Italy. Phone: 390862433542. Fax: 390862433523. E-mail: andrewreay.mackay@univaq.it.
† The first two authors contributed equally to this article.
▽ Published ahead of print on 29 June 2009.

(GN) (37), suggesting that the intracellular localization of TrkAIII is a critical determinant of both differential signaling and oncogenic potential.

Intracellular nonnuclear membranes are separated into the endoplasmic reticulum (ER), ER-GN intermediate compartment (ERGIC), GN, and transport vesicles, which assemble around, integrate, and interact with the centrosome (38). The centrosome, comprised of two centrioles embedded within a pericentriolar matrix of over 100 proteins, including γ-tubulin, acts as the major microtubule-organizing center and orchestrates the assembly, organization, and integration of the ER, ERGIC, GN, and associated vesicles (38). The centrosome also maintains genomic integrity by duplicating once per cell cycle S phase, ensuring bipolar mitotic spindle formation, accurate chromosome segregation, and the inheritance of a single centrosome by each daughter cell (23).

Centrosome duplication is tightly regulated by protein kinases Aurora-A and -B, polo kinases 1 and 4 (Plk-1 and Plk-4), Cdk2, PI3K, Zyg-1, Syk, Nek2, regulators Pin-1 and separase, and related phosphatases (11, 12, 18, 31, 42, 47, 53). The deregulation of centrosome duplication leads to centrosome amplification and subsequently to aberrant mitotic spindle formation, which promotes aneuploidy and polyploidy. These manifestations of genetic instability represent hallmarks of malignancy and drive tumor progression by promoting a more malignant phenotype (11, 12, 26, 35, 49). Centrosome amplification and subsequent genetic instability are induced by kinases that target the centrosome, the loss of centrosome-associated kinase inhibitors, altered levels of centrosome-associated regulators, and oncosuppressor inactivation (6, 7, 11, 12, 35, 40, 42, 49, 53).

The localization of TrkAIII to internal membranes, as a prerequisite for oncogenic activity (44, 45), makes identification of the membrane context within which TrkAIII exhibits activity and novel substrate interactions within this environment important in elucidating how TrkAIII exerts oncogenic potential. In the present study, we unveil a novel oncogenic mechanism for TrkAIII by demonstrating that TrkAIII activation within membranes that associate closely with the assembled ER/ERGIC/GN facilitates recruitment to the centrosome, results in centrosome amplification, and promotes genetic instability.

## MATERIALS AND METHODS

**Cell lines and expression vectors.** TrkAI and TrkAIII expression vectors andstably pcDNA-, TrkAI-, and TrkAIII-transfected SH-SY5Y and NIH 3T3 cell lines have been described previously (44). Green fluorescent protein (GFP)-centrin-expressing HeLa cells (34) were supplied by L. Di Marcotullio (University of Rome La Sapienza). Cell lines were grown in recommended medium (RPMI or Dulbecco's modified Eagle's medium), supplemented with 10% fetal calf serum and appropriate antibiotics (phleomycin [Zeocin], penicillin, and streptomycin). The kinase-dead mutant kd-$_{mu}$TrkAIII pcDNA3.1Zeo expression vector bearing phenylalanine substitutions of *tk* loop tyrosines Y670, Y674, and Y675, was constructed from the pcDNA TrkAIII (44) by replacing a 370-bp EcoRV digestion fragment with a PCR product generated using the Y670F/Y674F/Y675F mutant forward primer 5′-AGCAGGGATATCTtCAGCACCGACTttTtCCGTGTG-3′ and the reverse primer 5′-GCCACTGTGCTGGATATCTGCAGAATTC-3′ (lowercase letters indicate mutated nucleotides). SH-SY5Y cells stably transfected with kd-$_{mu}$TrkAIII were obtained as previously described for the generation of stably TrkAI- and TrkAIII-transfected SH-SY5Y cells (44).

**Reagents and antibodies.** Cell culture reagents, sodium orthovanadate, brefeldin A (BFA), geldanamycin (GA), cytochalasin D, nocodazole (NZ), SCH-58621, proteinase inhibitor cocktail, bis-benzimide trihydrochloride, propidium iodide, iohexol (Histodenz), nerve growth factor (NGF), polyclonal anti-ERGIC53, anti-γ-tubulin, and anti-NGF-neutralizing antibodies were from Sigma-Aldrich (St. Louis, MO). The pan-Trk inhibitor CEP-701 (4) was supplied by Cephalon Inc. (West Chester, PA), and the c-Src inhibitor GCP77675 was from Novartis Pharma (28). Anti-human Cep170 antibody was supplied by G. Guarguaglini (University of Rome La Sapienza, Rome, Italy) (14). The monoclonal anti-α-tubulin, anti-phosphotyrosine (pY99), and anticalnexin antibodies and the polyclonal anti-carboxyl terminal TrkA (C14) and anti-phospho-Y490 TrkA antibodies were from Santa Cruz Biotechnology (Santa Cruz, CA). The monoclonal anti-human extracellular domain TrkA antibody MRG12 was from Alexis Biochemicals (Plymouth Meeting, PA). The polyclonal antiactin, anti-TGN46, and antiseparase antibodies and monoclonal anti-Nedd-1 and anti-GMAP-210 antibodies were from Abcam (Cambridge, United Kingdom). The monoclonal anti-mannosidase II antibody was from Novus Biologicals (Littleton, CO), monoclonal anti-GM130 antibody was from BD Bioscience (San Jose, CA), and polyclonal anti-Plk4 antibody was from Cell Signaling (Danvers, MA). Fluorescein isothiocyanate- and Texas Red-conjugated secondary anti-mouse and anti-rabbit IgG antibodies were from Jackson ImmunoResearch (Bar Harbor, ME).

**RT-PCR conditions and primers.** Reverse transcription (RT) reactions were performed using mRNA (1 μg) and a Moloney murine leukemia virus reverse transcriptase kit according to the manufacturer's instructions (Life Technologies, Inc., Paisley, United Kingdom), in a final volume of 20 μl for 45 min at 42°C. Aliquots (1 μl) of diluted RT reaction mix were subjected to 35 cycles (1 min at 94°C, 1 min at 55°C, and 2 min at 72°C) of PCR amplification using the following specific primers: for TrkAI/TrkAII and TrkAIII, forward primer 5′-AACCTCACCATCGTGAAGAGTGGT-3′ and reverse primer 5′-GGTTGAACTCGAAAGGGTTGTCCA-3′; for Plk-4, forward primer 5′-GCCAAGGACCTTATTCACCAGT-3′ and reverse primer 5′-GTTGGCATTGTTGTCTGTGGGT-3′; for XBP-1, forward primer 5′-TTACGAGAGAAAACTCATGGC-3′ and reverse primer 5′-GGGTCCAAGTTGTCCAGAATGG-3′; and for glyceraldehyde-3-phosphate dehydrogenase (GAPDH), forward primer 5′-CGGAGTCAACGGATTTGGTCGTAT-3′ and reverse primer 5′-AGCCTTCTCCATGGTGGTGAAGAC-3′. These primers were used to control RNA quality and quantity. RT-PCR products were resolved by 1.5% agarose gel electrophoresis.

**Ultracentrifugation of intracellular membranes.** Intracellular nucleus-free membranes were purified from exponentially growing SH-SY5Y transfectants and separated into ER and non-ER fractions as previously described (52). Briefly, cells were washed and scraped into cold PBS, washed in homogenization buffer (130 mM KCl, 5 mM $MgCl_2$, 25 mM Tris-HCl, pH 7.3), and homogenized in 500 μl homogenization buffer containing proteinase inhibitor cocktail [1 mM 4-(2-amino-ethyl)benzenesulfonylfluoride hydrochloride, 20 μM leupeptin, 15 μM pepstatin, 15 μM chymostatin]. Homogenates were centrifuged for 5 min at 1,000 × *g* at 4°C, and supernatants were collected and recentrifuged at 1,000 × *g* for 5 min at 4°C to give the postnuclear supernatant. The postnuclear supernatant was adjusted to 500 μl in homogenization buffer and layered on top of a step gradient composed, from bottom to top, of 500 μl of 40%, 1 ml of 20% iohexol, 1 ml of 17.5% iohexol, and 1 ml of 15% iohexol (Sigma-Aldrich), diluted in homogenization buffer. Gradients were subjected to ultracentrifugation at 4°C in an SW 55 Ti rotor for 60 min at 100,000 × *g*, and 500-μl fractions, collected from top to bottom, were mixed with 125 μl of 5× detergent buffer (5% NP-40, 2.5% deoxycholate, 0.5% sodium dodecyl sulfate [SDS], 250 mM Tris-HCl, pH 8.0) and either subjected to immunoprecipitation (IP) with anti-TrkA (C14) antibody or separated by Western blotting to identify fractions positive for the GN and ER markers as previously described (52). Immunoprecipitates were washed once with radioimmunoprecipitation assay buffer (1% NP-40, 0.5% deoxycholate, 0.1% SDS, 150 mM NaCl, 50 mM Tris-HCl, pH 8.0), two times with high-salt buffer (0.2% SDS, 1% Triton X-100 [TX100], 5 mM EDTA, 500 mM NaCl, 50 mM Tris-HCl, pH 8.0), and once with TEN buffer (50 mM Tris-HCl, pH 8.0, 5 mM EDTA, 150 mM NaCl), prior to analysis by reducing SDS-polyacrylamide gel electrophoresis (PAGE)/Western blotting.

**Rabbit enolase kinase assay.** Kinase assays were performed as previously described (25). Briefly, acid-denatured rabbit muscle enolase (5 μg; Sigma) was added as the substrate to 50 μl of reaction buffer (10 mM HEPES, pH 7.4, 5 mM $MgCl_2$, 10 μM ATP, 100 μM sodium orthovanadate) containing 10 to 20 μCi [γ-$^{32}$P]ATP (Amersham) and anti-TrkA IP products. Reaction mixes were incubated at 30°C for 15 min, and reactions were terminated by the addition of 50 ml of 2× SDS-PAGE sample buffer (120 mM Tris, pH 6.8, 20% glycerol, 2% SDS) containing 100 mM dithiothreitol. Samples were heated to 90°C and subjected to 10% SDS-PAGE. Dried gels were exposed to Kodak XAR film with an intensifying screen at −70°C for a minimum of 7 days.

**Sucrose density gradient ultracentrifugation purification of centrosomes.** Briefly, cells were preincubated with cytochalasin D (1 μg/ml) and NZ (0.1 μM) for 1 h at 37°C and then harvested by trypsinization. Harvested cells ($1 \times 10^7$ to $3 \times 10^7$) were washed in phosphate-buffered saline (PBS) and lysed in 5 ml of

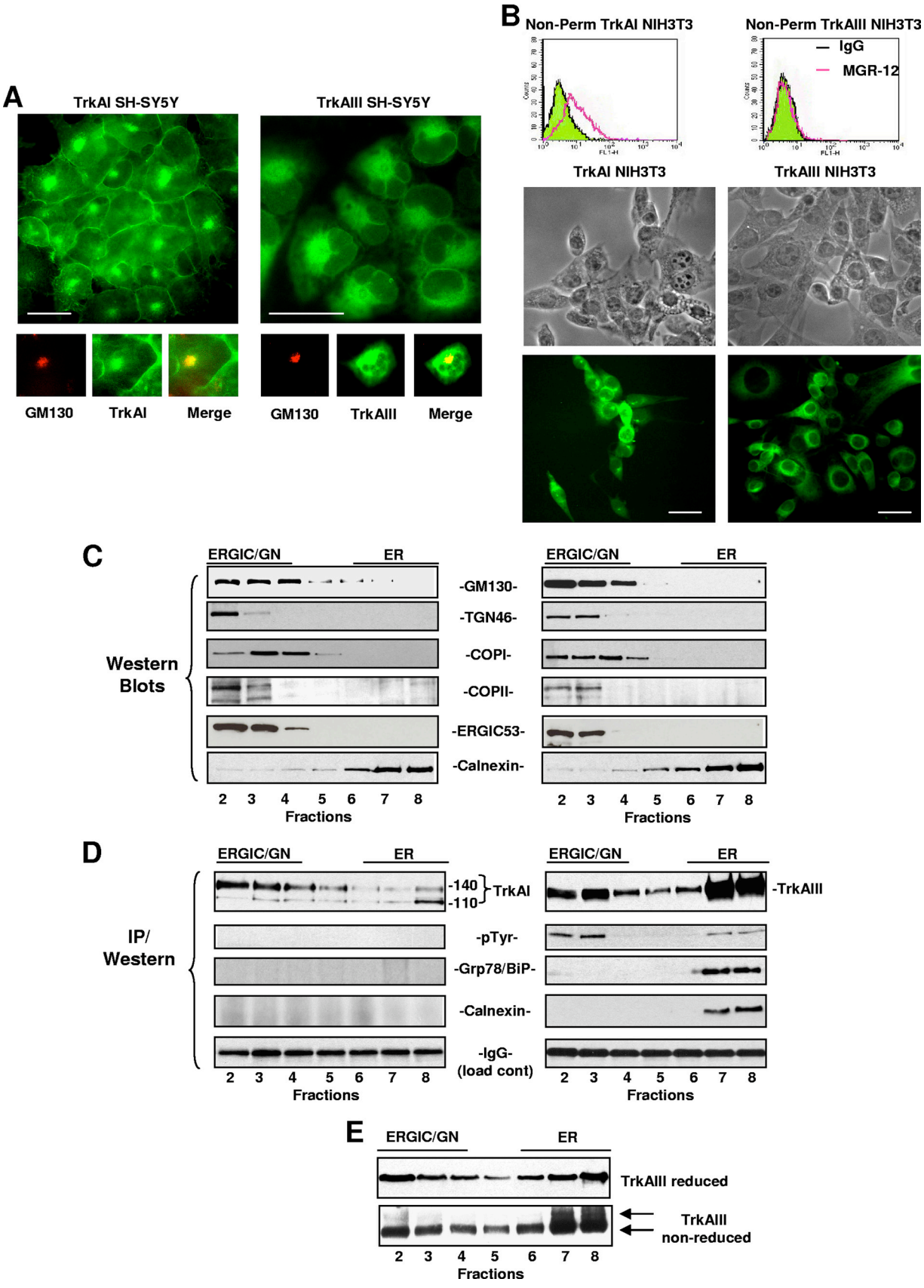

lysis buffer (1 mM HEPES, pH 7.2, 0.5% NP-40, 0.5 mM $MgCl_2$, 0.1% 2-mercaptoethanol) containing EDTA-free proteinase inhibitor cocktail (Boeringer Mannheim) and the phosphatase inhibitors sodium fluoride (50 mM) and sodium orthovanadate (1 mM). Swollen nuclei and chromatin aggregates were removed by centrifugation at 2,500 × *g* for 10 min at 4°C, and supernatants were filtered through 40-μm mesh nylon filters. Supernatants were adjusted to 10 mM HEPES, 2 U/ml DNase I (Boeringer Mannheim) was added, and the supernatants were incubated on ice for 30 min. Lysates were underlaid with 500 μl of 60% sucrose solution in 10 mM PIPES [piperazine-*N*,*N*′-bis(2-ethanesulfonic acid), pH 7.2], 0.1% Triton X-100, and 0.1% 2-mercaptoethanol, and centrosomes were sedimented into the sucrose cushion by centrifugation at 10,000 × *g* for 30 min at 4°C. The bottom 1.5 ml of the sucrose cushion was taken, resuspended, and overlaid onto a discontinuous gradient composed of 500 μl of 70% sucrose, 300 μl of 50% sucrose, and 300 μl of 40% sucrose solution in the aforementioned diluent. Gradients were ultracentrifuged at 120,000 × *g* for 1 h at 4°C, and seven 200-μl fractions were taken from bottom to top, with the remaining 1 ml taken as fraction 8. Each fraction was diluted to 1 ml with 10 mM PIPES buffer (pH 7.2) and centrifuged at 15,000 × *g* for 10 min at 4°C. Reducing SDS-PAGE sample buffer was added to pellets, and each fraction was subjected to SDS-PAGE/Western blotting. Anti-γ-tubulin antibody was used to identify centrosome-containing fractions as previously described (42).

**GFP-centrin-expressing HeLa cell centrosome amplification assay.** Stably GFP-centrin-transfected HeLa cells ($5 \times 10^4$) (34), were seeded onto Nunc glass chamber slides (Sigma-Aldrich, MO) and grown for 24 h to 50% confluence prior to transient transfection with 1 μg expression vector in 3 μl of Fugene-6 transfection reagent (Invitrogen, San Giuliano, Italy) for 6 h at 37°C. At 6 h, transfection medium was replaced with complete culture medium and cells grown for a further 48 h at 37°C. At 48 h, cultures were washed in prewarmed PBS and incubated for 1 h at 37°C in PBS containing 5 μg/ml Hoechst 33342 (Sigma-Aldrich). Slides were rinsed in PBS, fixed in 10% formalin, and permeabilized in 100% cold methanol for 6 min at −20°C. Nonspecific binding sites were blocked in 1% bovine serum albumin in PBS–0.03% TX100 for 30 min, and slides were incubated for 2 h with primary anti-TrkA antibody (C14) diluted in blocking solution, rinsed in PBS–0.03% TX100, and then incubated for 1 h in secondary affinity-purified Texas Red-conjugated goat anti-rabbit IgG (Jackson ImmunoResearch) diluted in blocking solution, as recommended by the manufacturer. Following incubation, slides were washed in PBS–0.03% TX100 and mounted in VectorMount and examined under a Zeiss Axioplan 2 fluorescence microscope, armed with a digital camera system and Leica M500 Image Manager software.

**TrkAIII PNA synthesis.** Fmoc (9-fluorenylmethoxy carbonyl; benzhydryloxycarbonyl) peptide nucleic acid (PNA) monomers were from (PRIMM, Milan, Italy); amino acids, activators, and resins were from Novabiochem (Nottingham, United Kingdom); acetonitrile was from Riedel-deHaën (Seelze, Germany); and dry *N*,*N*-dimethylformamide (DMF) was from Lab-Scan (Stillorgan, Ireland). All other reagents were from Fluka (St. Louis, MO). Solid-phase PNA synthesis was performed on an Expedite 8909 nucleic acid synthesis system (ABI). Liquid chromatography-mass spectrometry analyses were performed on a Thermo Finnigan liquid chromatography-mass spectrometry system with an electrospray source (MSQ) on a Phenomenex Jupiter 5-μm $C_{18}$ 300-Å (150- by 4.6-mm) column. A Phenomenex Jupiter 10-μm Proteo 90-Å (250- by 10-mm) column was used for purification on a semipreparative scale. Peptides were synthesized on a phenylalanine ammonia lyase-polyethylene glycol resin (0.16 mol/g). Briefly, amino acids (10 eq) were preactivated in 1-hydroxy benzotriazole–*N*-[(1H-benzitriazol-1yl)(dimethylamino)methylene]-*N*-methylmethanaminium hexafluorophosphate *N*-oxide (9.8 eq; 0.5 M) in DMF and *N*,*N*-diisopropylethylamine (DIPEA) (30 eq) and coupled for 15 min. The resin was washed with DMF (two flow washes, 25-s each), and capping was performed in acetic anhydride-DIPEA-DMF (15:15:70, vol/vol/vol) for 5 min, followed by two 25-s flow washes with DMF. Peptides were deprotected in piperidine-DMF (20:80, vol/vol) for 5 min, and resin was washed with DMF (two flow washes, 25-s each) and transferred into a small reaction vessel for PNA oligomer assembly. PNAs were synthesized on a 2-μmol scale in an Expedite 8909 synthesizer by using standard protocols. Double coupling was carried out on polypurine tracts (doubly coupled bases are underlined in the sequences). At the end of the synthesis, resins were washed with dichloromethane and vacuum dried. PNA and the peptide-PNA conjugates (16) were cleaved from the resin and deprotected in a solution of trifluoroacetic acid (TFA)–triisopropylsilane–*m*-cresol (78:2:20) for 90 min at room temperature to obtain KKAA-TrkAIII [$(KKAA)_4$-GGCCGGGACACA], which was purified by high-performance liquid chromatography in a 5-min gradient of 7% isocratic water (0.1% TFA), followed by a 30-min gradient of acetonitrile (0.1% TFA) in water (0.1% TFA) from 7 to 35%, eluted at 22.2 min, identified by electrospray mass analysis, and lyophilized three times to remove excess TFA.

**IP and Western blots.** Cells were extracted on ice in lysis buffer (PBS containing 0.5% sodium deoxycholate, 1% NP-40, 0.1% SDS, 1 mM sodium orthovanadate, 1 mM phenylmethylsulfonyl fluoride, 1 μg/ml of pepstatin A, aprotinin), and protein concentrations were calculated by the Bradford assay (Sigma-Aldrich). Extract aliquots (200 to 500 μg) were precleared with 1 μg of preimmune IgG (1 h at 4°C) and 20 μl of protein A Sepharose (Fast Flow; Sigma-Aldrich) for 20 min at 4°C and 200 to 500 μg of precleared extract incubated with primary antibody (0.1 to 1.0 μg antibody/500 μg protein extract) for 2 to 16 h at 4°C. Following incubation, 20 μl of protein A Sepharose (Fast Flow; Sigma-Aldrich) in lysis buffer was added, and reaction mixes were incubated for 30 min at 4°C. Protein A Sepharose-IgG conjugates were collected by centrifugation (10,000 × *g* for 5 min), washed three times in lysis buffer, resuspended in SDS-PAGE sample buffer, and subjected to reducing SDS-PAGE/Western blotting. Proteins, transblotted by electrophoresis onto Hybond C+ nitrocellulose membranes (Amersham International, United Kingdom), were air dried, and nonspecific protein binding sites were blocked by incubation for 2 h in 5% nonfat milk in Tris-buffered saline and membranes and then incubated with primary antibody at the recommended dilution in blocking solution for 2 to 16 h at 4°C. Blots were washed in Tris-buffered saline and incubated with secondary horseradish peroxidase-conjugated antibody diluted in blocking solution, and immunoreactive species were detected by a chemiluminescence reaction (Amersham International, Bedford, United Kingdom).

**Cell cycle and cell surface TrkA fluorescence-activated cell sorter (FACS) analysis.** Cells were recovered, washed twice in ice-cold PBS, and fixed in 70% ethanol at 4°C for at least 30 min, washed twice in ice-cold PBS, stained with 50 μg/ml of propidium iodide solution containing 25 μg/ml of RNase A and incubated in the dark at room temperature for 30 min. Cell cycle phase distribution was analyzed by flow cytometry (FACScan flow cytometry; Becton Dickinson Immunocytometry Systems, San Jose, CA), and data from 10,000 events per sample were analyzed using Modfit LT for Mac version 3.0 cell cycle analysis software. For cell surface TrkA expression in nonpermeabilized cells, cells were detached at 4°C with PBS-EDTA, resuspended in calcium and magnesium-free PBS, dispersed into 12 75-mm tubes ($0.5 \times 10^6$ cells per tube), centrifuged, and incubated with 0.5 μg of anti-TrkA MGR12 monoclonal antibody or 0.5 μg of normal mouse IgG in 100 μl PBS at 4°C for 1 h. After being washed with PBS, cells were incubated with fluorescein isothiocyanate-conjugated goat anti-mouse IgG (Sigma; diluted 1:128 in PBS) at 4°C for 45 min, washed in PBS, resuspended in 500 μl PBS, and analyzed in a FACScan analyser (Becton Dickinson).

FIG. 1. TrkAIII differs from TrkAI in intracellular membrane distribution. (A) Indirect IF demonstrating TrkAI (green, upper-left panel) and TrkAIII (green, upper-right panel) expression in respective stably transfected SH-SY5Y cells; GM130 (red), TrkAI (green), and merged TrkAI/GM130 (orange/yellow) expressions in a representative TrkAI SH-SY5Y transfectant (three lower-left panels) and GM130 (red), TrkAIII (green), and merged TrkAIII/GM130 (orange/yellow) expressions in a representative TrkAIII SH-SY5Y transfectant (three lower-right panels). Bar = 50 μm. (B) FACS analysis demonstrating cell surface immunoreactivity of nonpermeabilized (nonperm) TrkAI but not nonpermeabilized TrkAIII NIH 3T3 transfectants to MGR-12 anti-TrkA monoclonal antibody (pink line) relative to immunoreactivity to preimmune IgG (black line). Phase-contrast micrographs (middle two panels) comparing morphologies plus indirect IF (bottom panels) comparing TrkAI and TrkAIII expressions (green) in respective TrkAI and TrkAIII NIH 3T3 transfectants. Bar = 50 μM. (C) Western blots demonstrating GM130, TGN46, COP I, COP II, ERGIC53, and calnexin distributions in ultracentrifugation-fractionated intracellular nonnuclear membranes from TrkAI (left panels) and TrkAIII (right panels) SH-SY5Y transfectants. (D) IP/Western blots demonstrating the distributions of TrkAI and TrkAIII, phosphorylation statuses, and coimmunoprecipitations of Grp78/BiP and calnexin in ultracentrifugation-fractionated membranes from TrkAI (left panels) and TrkAIII (right panels) SH-SY5Y transfectants. IgGs in immunoprecipitates are shown as loading controls. (E) IP/Western blots demonstrating alternatively folded TrkAIII (arrow) in calnexin-positive ER fractions (lanes 7 and 8) under nonreducing conditions (lower panel) but not under reducing conditions (upper panel).

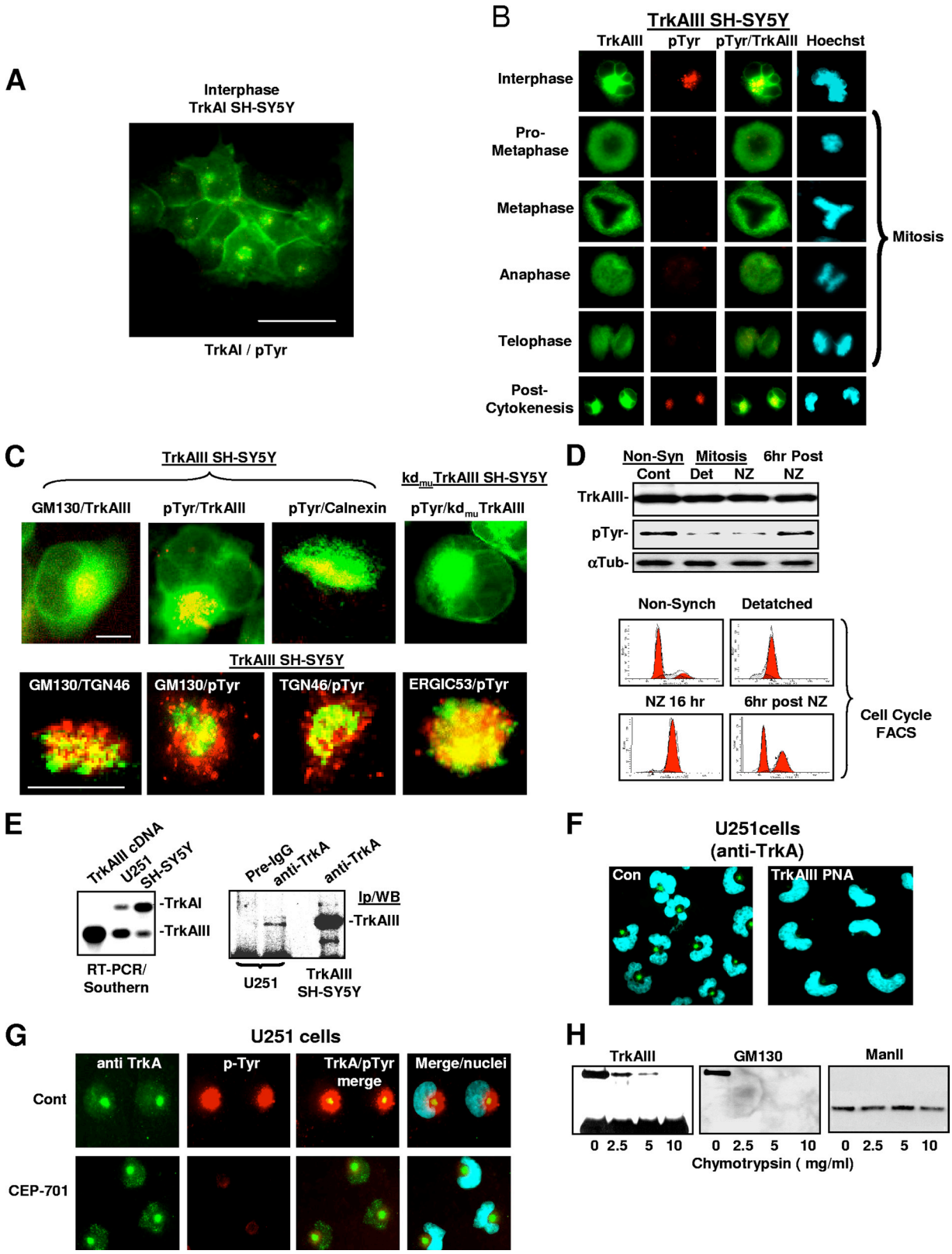


FIG. 2. TrkAIII is activated during interphase within ER/ERGIC/GN-associated structures. (A) Indirect IF demonstrating no tyrosine phosphorylation (pTyr; not detected) associated with TrkAI (green) in interphase TrkAI SH-SY5Y transfectants (bar = 50 μm). (B) Indirect IF demonstrating TrkAIII expression (green), tyrosine phosphorylation (red; pTyr), merged pTyr/TrkAIII expression (orange/yellow), and Hoechst-stained chromatin (light blue) in SH-SY5Y transfectants during interphase, prometaphase, metaphase, anaphase, telophase, and postcytokinesis. (C) The top panels show indirect IF demonstrating merged (yellow/orange) GM130 (red) and TrkAIII (green) expression (leftmost panel),

**IF.** Cells grown on Nunc glass chamber slides (Sigma-Aldrich) were washed in PBS, fixed in 96% ethanol–3% glacial acetic acid, and processed for indirect immunofluorescence (IF). Slides were incubated for 1 h in blocking solution (1% bovine serum albumin in PBS–0.03% TX100) and then for 2 to 16 h with primary antibody in blocking solution at room temperature. Slides were washed three times in PBS–0.03% TX100, then incubated with secondary fluorochrome-conjugated antibody diluted in blocking solution for 1 h at room temperature, and then washed in PBS–0.03% TX100 and mounted using VectorMount. IF images were obtained using a Zeiss Axioplan 2 fluorescence microscope with a digital camera and Leica M500 Image Manager software.

**Metaphase spreads and SCE.** Cells treated for 2 h with colcemid (0.5 μg/ml) (Sigma-Aldrich, MO) were harvested by trypsinization, and metaphase spreads were prepared by swelling in hypotonic KCl solution (0.57%) for 10 min at 37°C. After treatment, the cells, fixed in 3:1 methanol-acetic acid, were washed twice in fresh fixative, and aliquots were dropped onto glass sides and air dried. For sister chromatid exchange (SCE), cells were grown in the presence of 10 μM 5-bromodeoxyuridine (Sigma-Aldrich) in the dark for 48 h prior to colcemid treatment and processed as described above, with the exception that air-dried slides were aged for 3 days. Aged slides were incubated with 5 μg/ml Hoechst 33258 (Sigma-Aldrich) for 10 min, rinsed in water, air dried, covered with 2× SSC (1× SSC is 0.15 M NaCl plus 0.015 M sodium citrate; pH. 7), and irradiated with a mixture of long- and short-wave UV light at a distance of 20 cm for 2 h in the dark at room temperature. Slides were then incubated in 2× SSC (pH 7) for 2 h at 60 to 65°C, rinsed in water, and air dried. Air-dried slides were stained with 2% Giemsa stain for 15 min, rinsed in water, air dried, passed through xylene, and mounted in Depex medium. Metaphase spreads and SCE were assessed by light microscopy using a Zeiss Axioplan 2 microscope with a digital camera and Leica M500 Image Manager software.

## RESULTS

**TrkAIII localizes to ER/ERGIC/GN membranes.** Indirect IF demonstrated predominant expression of TrkAI at the cell surface and within the GN in stable TrkAI SH-SY5Y transfectants (Fig. 1A, upper-left panel). The GN localization of TrkAI was confirmed by overlapping expression with the *cis*-GN marker GM130 (Fig. 1A, lower-left panels). In contrast to TrkAI, TrkAIII expressed by stable TrkAIII SH-SY5Y transfectants was not detected at the cell surface and accumulated within the intracellular compartment (Fig. 1A, upper-right panel) (44) but did not localize exclusively to the GM130-positive GN (Fig. 1A, lower-right panels). For nonpermeabilized stable NIH 3T3 transfectants, FACS analysis using an anti-TrkA extracellular domain monoclonal MGR12 specific for both TrkAI and TrkAIII, which detects cell surface TrkAI but not TrkAIII in stable SH-SY5Y transfectants (45), also confirmed cell surface TrkAI but not TrkAIII expression (Fig. 1B, top panels). Cell surface TrkAI expression in NIH 3T3 transfectants detected by indirect IF was less evident at intercellular junctions than that detected in SH-SY5Y transfectants (compare Fig. 1B, lower-left panel, and A, upper-left panel). This may reflect the high degree of intercellular association exhibited by SH-SY5Y cells (Fig. 1A) relative to that exhibited by NIH 3T3 cells (Fig. 1B, lower four panels), which concentrates cell surface TrkAI to intercellular junctions, facilitating detection (Fig. 1A). Alternatively, less TrkAI may reach the NIH 3T3 cell surface. Indirect IF also detected similarity in intracellular GN-localized TrkAI in SH-SY5Y transfectants (Fig. 1A, lower-left panels) and centralized concentrations of intracellular TrkAI in NIH 3T3 transfectants (Fig. 1B, lower-left panel), consistent with similar GN localization. Indirect IF also confirmed similarity in the less-centralized intracellular expression of TrkAIII in SH-SY5Y and NIH 3T3 transfectants (Fig. 1A, upper-right panel, and B, bottom-right panel). Other than exhibiting differences in nuclear morphology, TrkAI and TrkAIII NIH 3T3 transfectants did not differ appreciably in phase-contrast morphology (Fig. 1B, middle two panels). We confirm our previous report that TrkAI does not exhibit constitutive tyrosine phosphorylation in either SH-SY5Y or NIH 3T3 cells, whereas TrkAIII exhibits constitutive tyrosine phosphorylation in both SH-SY5Y and NIH 3T3 transfectants (44).

Ultracentrifugation-fractionated intracellular membranes from stable TrkAI SH-SY5Y transfectants characterized by Western blotting for the ER marker calnexin, *cis*-GN marker GM130, *trans*-GN marker TGN46, ERGIC marker ERGIC53, and coatamer vesicle markers COP I and COP II (Fig. 1C, left panel) were subjected to TrkAI IP. As shown in Fig. 1D (left panel), low levels of predominantly immature gp110 TrkAI characterized calnexin-positive ER membranes, whereas relatively higher levels of predominantly mature gp140 TrkAI characterized calnexin-negative non-ER membranes positive for ERGIC53, GM130, TGN46, COP I, and COP II. This indicates that TrkAI is not retained within the ER but readily exits to the ERGIC/GN/vesicle compartments in association with gp140 TrkAI maturation.

TrkAIII immunoprecipitated from fractionated intracellular SH-SY5Y membranes exhibited relatively high-level retention and tyrosine phosphorylation within both calnexin-positive ER



TrkAIII (green) and tyrosine phosphorylation (red; pTry) (second panel), and calnexin (green) and tyrosine phosphorylation (red; pTyr) (third panel) in representative interphase TrkAIII SH-SY5Y transfectants, plus a lack of merge between tyrosine phosphorylation (pTyr; not detected) and kd-$_{mu}$TrkAIII (green) (fourth panel) in an interphase kd-$_{mu}$TrkAIII SH-SY5Y transfectant. The lower panels demonstrate merged (yellow/orange) GM130 (green) and TGN46 (red) expression (leftmost panel), GM130 (green) and tyrosine phosphorylation (red; pTyr) (second panel), TGN46 (green) and tyrosine phosphorylation (red; pTyr) (third panel), and ERGIC53 (green) and tyrosine phosphorylation (red; pTyr) (fourth panel) in representative interphase TrkAIII SH-SY5Y transfectants. Bar = 10 μm. (D) IP/Western blots demonstrating reduced TrkAIII tyrosine phosphorylation relative to total TrkAIII and α-tubulin in extracts from TrkAIII SH-SY5Y transfectants synchronized in $G_2$/M by detachment (Det) or 16-h NZ treatment (NZ), compared to unsynchronized controls (Non-Syn Cont) and cells 6 h post-NZ release (cell cycle FACS analyses are provided for each cell population in the lower panels). (E) RT-PCR/Southern blot (left panel) demonstrating predominant endogenous TrkAIII over TrkAI/II mRNA expression in U251 compared to SH-SY5Y cells, plus an IP/Western blot (right panel) demonstrating predominant endogenous TrkAIII expression in U251 cells and TrkAIII SH-SY5Y transfectants. (F) Indirect IF demonstrating endogenous TrkAIII expression in nonstressed U251 cells (Con, green) and inhibition of endogenous TrkAIII expression by 7-day treatment with 10 μM TrkAIII-PNA (Hoechst-stained nuclei are light blue). (G) Indirect IF demonstrating endogenous TrkAIII expression (green, upper and lower leftmost panels), tyrosine phosphorylation (red; pTyr, upper and lower second panels); merged TrkAIII expression and tyrosine phosphorylation (orange/yellow, upper and lower third panels) plus merged TrkAIII expression, tyrosine phosphorylation, and Hoechst-stained nuclei (light blue) (upper and lower fourth panels) in untreated (Cont, upper panels) and 100 nM CEP-701-treated (CEP-701, lower panels) U251 cells. (H) IP/Western blots demonstrating loss of TrkAIII carboxyl-terminal domain and GM130 but not mannosidase II immunoreactivity in purified ERGIC/GN membranes incubated for 10 min at 4°C with chymotrypsin at the concentrations indicated.

membranes and calnexin-negative non-ER membranes positive for ERGIC53, GM130, TGN46, and COP I/II (Fig. 1D, right panel). Furthermore, TrkAIII associated with calnexin-positive ER membranes coimmunoprecipitated the ER chaperones calnexin and Grp78/BiP (Fig. 1D, right panel) and exhibited alternative folding with an additional 105-kDa TrkAIII species detected under nonreducing conditions but not under reducing conditions (Fig. 1E). TrkAIII expression, however, did not associate with constitutive alternative XBP-1 splicing (data not shown), indicating that TrkAIII does not activate the Ire1α branch of the ER stress response (51).

**TrkAIII in a cytoplasmic tk domain orientation exhibits interphase-restricted, ER/ERGIC/GN-associated activation.** In contrast to the case with TrkAI, which does not exhibit tyrosine phosphorylation despite significant GN accumulation (Fig. 2A), indirect IF using a general phosphotyrosine antibody (pTyr) detected TrkAIII-associated tyrosine phosphorylation during interphase and postcytokinesis but not during mitosis in SH-SY5Y transfectants (Fig. 2B). TrkAIII-associated tyrosine phosphorylation detected by indirect IF during interphase was localized primarily to vesicle-like structures at the center of the calnexin-positive ER (Fig. 2C, third panel from the left on the top row) in close, overlapping association with GM130, TGN46, and in particular, ERGIC53 (Fig. 2C, second, third, and fourth panels on the bottom row). SH-SY5Y transfectants synchronized in $G_2$/M by detachment (by FACS, 88% $G_2$/M, 2% $G_1$, and 10% S phase) and by 16-h NZ treatment (by FACS, 91% $G_2$/M, 1.3% $G_1$, and 7.7% S phase) also exhibited reduced TrkAIII tyrosine phosphorylation compared to unsynchronized counterparts (by FACS, 65% $G_1$, 14% $G_2$, and 21% S phase) and 6 h following NZ release (by FACS, 60% $G_1$ and 40% $G_2$/M), in IP/Western blots (Fig. 2D). In contrast to nonmutated TrkAIII, similar levels of intracellular expression of kd-$_{mu}$TrkAIII were not associated with tyrosine phosphorylation in SH-SY5Y cells (Fig. 2C, pTyr/kd-$_{mu}$TrkAIII panel), confirming that TrkAIII-associated tyrosine phosphorylation is TrkAIII tk dependent. Constitutive expression of endogenous TrkAIII mRNA detected by RT-PCR (Fig. 2E, left panel), as well as intracellular expression of endogenous TrkAIII protein detected by Western blotting (Fig. 2E, right panel) and indirect IF (Fig. 2F and G), characterized nonstressed human neural U251 glioma cells. Indirect IF detected TrkAIII-PNA (10 μM) inhibition of endogenous TrkAIII expression by U251 cells (Fig. 2F). Endogenous TrkAIII expression in U251 cells was associated with areas of intracellular tyrosine phosphorylation (Fig. 2G, upper panels), inhibited by 100 nM CEP-701 (Fig. 2G, lower panels). These data indicate that interphase-restricted TrkAIII activity within ER/ERGIC/GN-associated structures is not confined to conditions of exogenous overexpression.

Chymotrypsin digestion of fractionated ERGIC/GN membranes from TrkAIII SH-SY5Y transfectants eliminated membrane-associated TrkAIII carboxyl terminal and GM130 but not mannosidase II immunoreactivity (Fig. 2H). This indicates a cytoplasmic orientation for the TrkAIII carboxyl terminus containing the tk domain, as previously described for GN-associated GM130 but not mannosidase II (52).

**TrkAIII binding of γ-tubulin is tk dependent and results in recruitment to the centrosome.** To further study TrkAIII tk function, a kd-$_{mu}$TrkAIII expression vector bearing phenylalanine substitutions of tk loop tyrosines Y670, Y674, and Y675 was constructed and stably transfected into SH-SY5Y cells. Like its nonmutated counterpart, 100-kDa kd-$_{mu}$TrkAIII exhibited intracellular expression and not cell surface expression in SH-SY5Y cells (Fig. 2C, fourth panel on the top row) but did not exhibit constitutive tyrosine phosphorylation assessed by indirect IF (Fig. 2C, compare second and fourth panels on the top row) or IP/Western blotting (Fig. 3A, upper and middle panels). In contrast to nonmutated TrkAIII, kd-$_{mu}$TrkAIII immunoprecipitated from stable SH-SY5Y transfectants did not exhibit kinase activity in a rabbit muscle enolase kinase assay (25), confirming that it corresponds to a kinase-dead allele (Fig. 3A, lower panel).

In coimmunoprecipitation assays, TrkAIII coimmunoprecipitated γ-tubulin from whole-cell extracts (Fig. 3B) and ultracentrifugation-fractionated intracellular membranes from TrkAIII SH-SY5Y transfectants (Fig. 3C, lower panels, middle column). In contrast, nonphosphorylated TrkAI and kd-$_{mu}$TrkAIII coimmunoprecipitated negligible levels of γ-tubulin from whole-cell extracts (Fig. 3B), levels below the threshold of detection in ultracentrifugation-fractionated membranes (Fig. 3C, left and right columns). Tyrosine-phosphorylated TrkAIII but not TrkAI or kd-$_{mu}$TrkAIII also copurified with γ-tubulin-positive sucrose density gradient ultracentrifugation-fractionated centrosomes from respective stable transfectants (Fig. 3D), and γ-tubulin coimmunoprecipitated TrkAIII from centrosomes purified from TrkAIII transfectants (Fig. 3E). TrkAIII tk involvement in γ-tubulin binding, suggested by the negligible binding exhibited by nonphosphorylated TrkAI and kd-$_{mu}$TrkAIII, was confirmed using CEP-701, which inhibited TrkAIII tyrosine phosphorylation and binding of γ-tubulin, and using the protein tyrosine phosphatase (PTPase) inhibitor sodium orthovanadate (1 mM), which stimulated TrkAIII tyrosine phosphorylation and binding of γ-tubulin in coimmunoprecipitation assays (Fig. 3F). A requirement for full ERGIC/GN assembly for TrkAIII binding of γ-tubulin was supported using the ERGIC/GN-disrupting agent BFA (5 μg/ml) (43), which inhibited TrkAIII tyrosine phosphorylation and binding of γ-tubulin (Fig. 3F), and a role for Hsp90 was suggested using the Hsp90 inhibitor GA (1 μM) (33), which also reduced TrkAIII tyrosine phosphorylation and binding of γ-tubulin (Fig. 3F). Levels of TrkAIII tyrosine phosphorylation and binding of γ-tubulin were not influenced by NGF-neutralizing antibody (1 μg/ml), A2a adenosine receptor antagonist SCH58621 (0.1 μM) (8), or c-Src inhibitor GCP77675 (28), following treatment for up to 16 h (data not displayed). The centrosome origin of γ-tubulin was confirmed by coimmunoprecipitation of centrosome-associated Nedd-1 (24) but not GN-associated γ-tubulin-binding protein GMAP-210 (39) from centrosome preparations (Fig. 3E).

**TrkAIII phosphorylates centrosome components.** TrkAIII at the centrosome (Fig. 4A) was confirmed to exhibit tk function in Western blotting, which detected differential tyrosine phosphorylation of 100-kDa, 70-kDa, 60-kDa, 48-kDa, 38-kDa, and 33-kDa centrosome-associated proteins in TrkAIII SH-SY5Y transfectants compared to TrkAI SH-SY5Y transfectants (Fig. 4B, compare lanes 1 and 3). These differences were abrogated by overnight treatment of TrkAIII transfectants with 100 nM CEP-701 (Fig. 4B, compare lanes 3 and 4), in association with reduced levels of total and tyrosine-phosphorylated TrkAIII relative to γ-tubulin (Fig. 4B, lower panels, compare lanes 3 and 4). CEP-701 treatment of TrkAI SH-

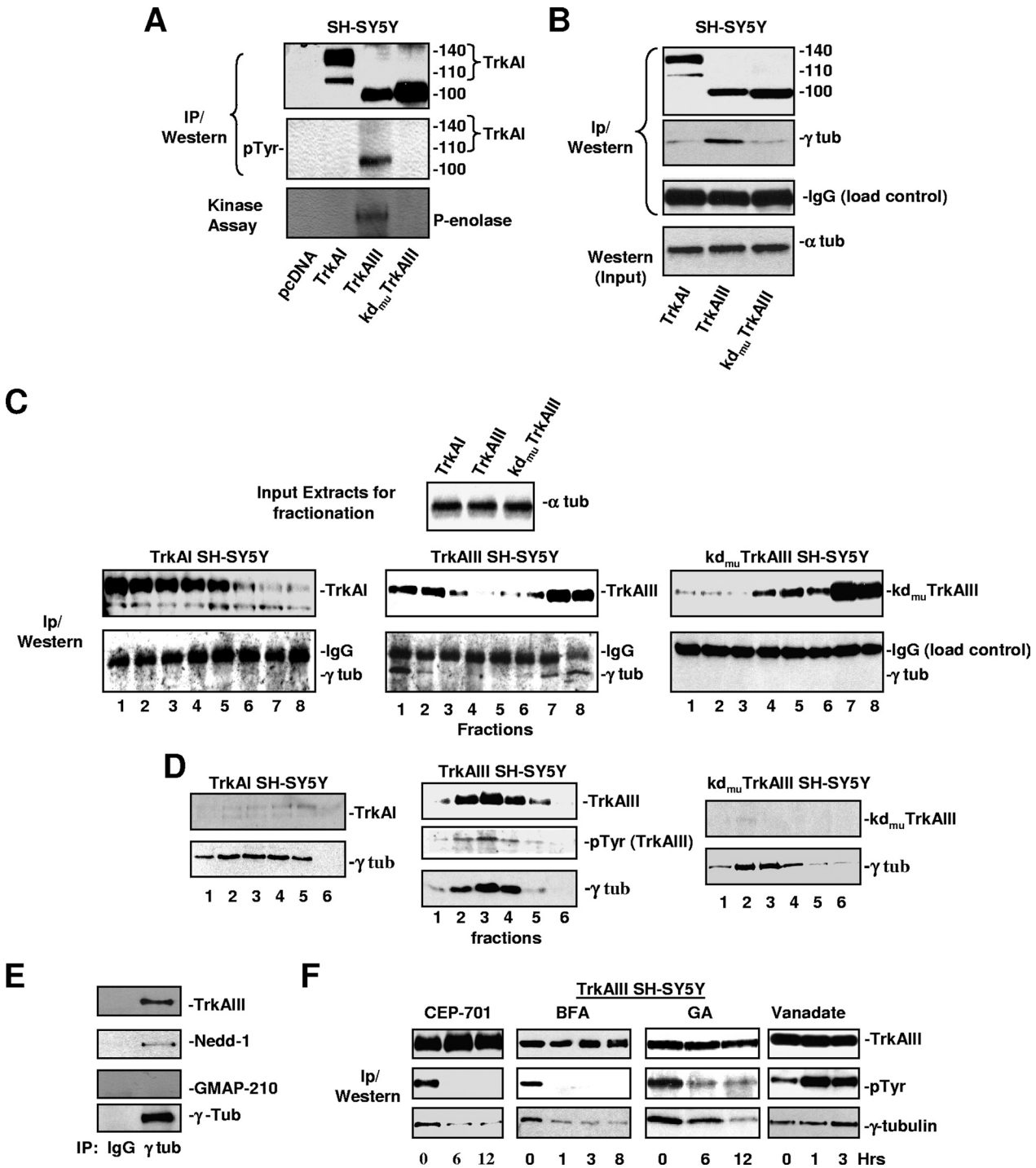


FIG. 3. TrkAIII interacts with the centrosome. (A) IP/Western blots (top and middle panels) demonstrating constitutive tyrosine phosphorylation (pTyr) associated with TrkAIII but not TrkAI or kd-$_{mu}$TrkAIII immunoprecipitated from respective SH-SY5Y transfectants, plus a representative rabbit enolase kinase assay (bottom panel) demonstrating phosphorylation of rabbit enolase by TrkAIII but not TrkAI or kd-$_{mu}$TrkAIII imunoprecipitate. (B) IP/Western blots demonstrating TrkAIII coimmunoprecipitation of γ-tubulin (γ tub) but negligible TrkAI and kd-$_{mu}$TrkAIII γ-tubulin coimmunoprecipitations from respective SH-SY5Y transfectants (relative α-tubulin [α tub] levels are displayed as input controls, and IgG levels in immunoprecipitates are displayed as a loading control). (C) IP/Western blots demonstrating TrkAIII but not TrkAI or kd-$_{mu}$TrkAIII coimmunoprecipitation of γ-tubulin from ultracentrifugation-fractionated nonnuclear membranes from respective SH-SY5Y transfectants (relative α-tubulin levels are displayed as input controls, and IgG levels in immunoprecipitates are displayed as a loading control). (D) Western blots demonstrating copurification of tyrosine-phosphorylated TrkAIII (middle panels) but not TrkAI (left panels) or kd-$_{mu}$TrkAIII (right panels) with γ-tubulin-positive sucrose density gradient-purified centrosomes from respective SH-SY5Y transfectants. (E) IP/Western blots demonstrating γ-tubulin coimmunoprecipitation of Nedd-1 and TrkAIII but not GMAP-210 from sucrose density gradient ultracentrifugation-purified centrosomes (fraction 3) from TrkAIII SH-SY5Y transfectants. (F) IP/Western blots demonstrating relative changes in TrkAIII tyrosine phosphorylation and coimmunoprecipitation of γ-tubulin in whole-cell extracts from TrkAIII SH-SY5Y transfectants treated with 100 nM CEP-701, 5 μg/ml BFA, 1 μM GA, or 1 mM sodium orthovanadate for the times indicated.

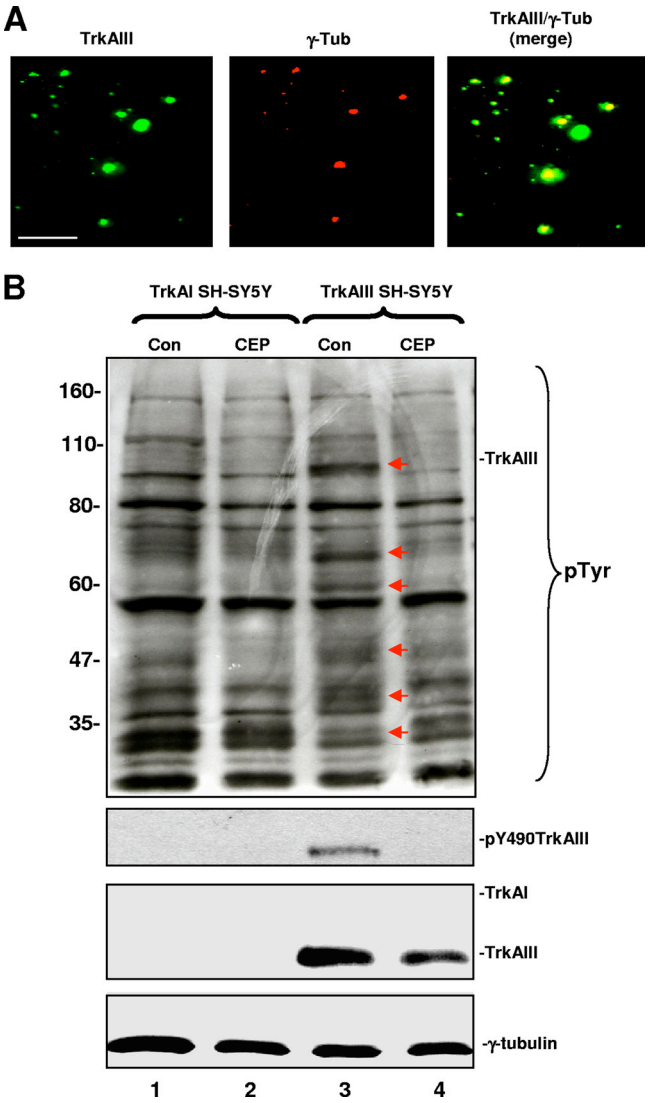


FIG. 4. TrkAIII tk phosphorylates centrosome components. (A) Indirect IF demonstrating TrkAIII (first panel from the left; green), γ-tubulin (γ Tub) (second panel; red), and merged TrkAIII/γ-tubulin expression (third panel; orange/yellow) in sucrose density gradient-purified centrosomes (fraction 3) from TrkAIII SH-SY5Y transfectants. Bar = 10 μm. (B) Western blots demonstrating differential (red arrows) centrosome component tyrosine phosphorylation (pTyr) in centrosomes purified from untreated (Con; lane 1) and 100 nM CEP-701-treated TrkAI SH-SY5Y transfectants (CEP; lane 2), compared to untreated (Con; lane 3) and 100 nM CEP-701-treated TrkAIII SH-SY5Y transfectants (CEP; lane 4). Lower panels demonstrate relative levels of Y490 tyrosine-phosphorylated TrkAIII, total TrkAIII, and γ-tubulin in the centrosome preparations.

SY5Y transfectants had little influence upon centrosome component tyrosine phosphorylation (Fig. 4B, compare lanes 1 and 2). Of the differentially phosphorylated proteins, TrkAIII is likely to represent the 100-kDa component. Differential phosphorylation of γ-tubulin was not detected despite TrkAIII binding (data not displayed). The remaining differentially phosphorylated centrosome proteins remain to be identified.

**TrkAIII increases Plk-4 levels at the centrosome.** Increased centrosome interaction with Plk-4 promotes rapid amplification of centrosomes (18). TrkAIII promotion of Plk-4 interaction with the centrosome was supported by (i) Plk-4 copurification with γ-tubulin-positive centrosome fractions from TrkAIII but not pcDNA or stable TrkAI SH-SY5Y transfectants, determined by Western blotting (Fig. 5A); (ii) the observation that TrkAIII but not TrkAI coimmunoprecipitated both Plk-4 and γ-tubulin from whole-cell extracts (Fig. 5B); and (iii) the observation that TrkAIII expression associated with an increased number of TrkAIII SH-SY5Y transfectants (24.2% ± 5.9%) exhibiting punctiform perinuclear Plk-4 staining (Fig. 5C), compared to pcDNA (11.8% ± 5.8%) and TrkAI (8% ± 2.9%) transfectants (six experiments, each representing 100 observations; *P* values of <0.005 for TrkAIII versus pcDNA and <0.001 for TrkAIII versus TrkAI transfectants; Student's *t* test) (Fig. 5D). Plk-4 expression in kd-$_{mu}$TrkAIII transfectants was not assessed.

**TrkAIII promotes centrosome amplification.** TrkAIII deregulation of centrosome duplication was confirmed by transient TrkAIII expression in human GFP-centrin-expressing HeLa cells (Fig. 6A) (34). In this model, GFP-centrin-expressing HeLa cells exhibited background centrosome amplification (>2 GFP-centrin-positive centrosomes per cell) in a mean (± standard deviation [SD]) of 12.5% ± 2.9% of cells (four independent experiments, each of 50 cells) (Fig. 6B, lane NT). Centrosome amplification was not increased above the background by transient pcDNA transfection or transient TrkAI expression and remained at 13.5% ± 3.9% in pcDNA and 15.5% ± 2.6% in TrkAI transient transfectants (Fig. 6B, lanes pcDNA and TrkAI, respectively). Transient TrkAIII expression significantly elevated centrosome amplification to 44% ± 8.3% in TrkAIII-positive transfectants (*P* values of <0.0001 for TrkAIII versus nontransfected and pcDNA- and TrkAI-transfected counterparts; Student's *t* test). This effect was abrogated in the presence of 100 nM CEP-701 (17% ± 2.9%) and 10 μM TrkAIII-PNA (16.5% ± 3.3%) (Fig. 6B, lanes TrkAIII CEP-701 and TrkAIII+PNA, respectively) and was not detected following transient expression of kd-$_{mu}$TrkAIII (15.1% ± 1.5%) (Fig. 6B). Mean centrosome numbers per cell in transient TrkAIII-GFP-expressing HeLa cell transfectants were not evaluated, due to the high levels of amplification detected, which made accurate counting difficult (Fig. 6A, bottom panels). These data show that TrkAIII promotes centrosome amplification.

Centrosome amplification in stably transfected cell lines, characterized by more than two γ-tubulin-positive centrosomes per cell (Fig. 6C), was detected in 14.2% ± 4.1% of stable pcDNA SH-SY5Y transfectants, 13.2% ± 4.62% of stable TrkAI SH-SY5Y transfectants, and 16.2% ± 2.8% of stable kd-$_{mu}$TrkAIII SH-SY5Y transfectants and was significantly elevated to 31.8% ± 5.8% in stable TrkAIII SH-SY5Y transfectants (six experiments, each consisting of 100 cells) (*P* value of <0.001 for TrkAIII versus pcDNA, TrkAI, and kd-$_{mu}$TrkAIII transfectants; Student's *t* test) (Fig. 6D).

The mean (± SD) number of centrosomes per cell for TrkAIII transfectants was 3.59 ± 2.8, with 32% of cells exhibiting >2 centrosomes. This was significantly elevated over the number of stable TrkAI transfectants (2.54 ± 1.64), with 15% of cells exhibiting >2 centrosomes per cell; pcDNA transfectants (2.5 ± 1.6), with 14% of cells exhibiting >2 centrosomes; and stable kd-$_{mu}$TrkAIII transfectants (2.76 ± 2.15), with 16% of cells ex-

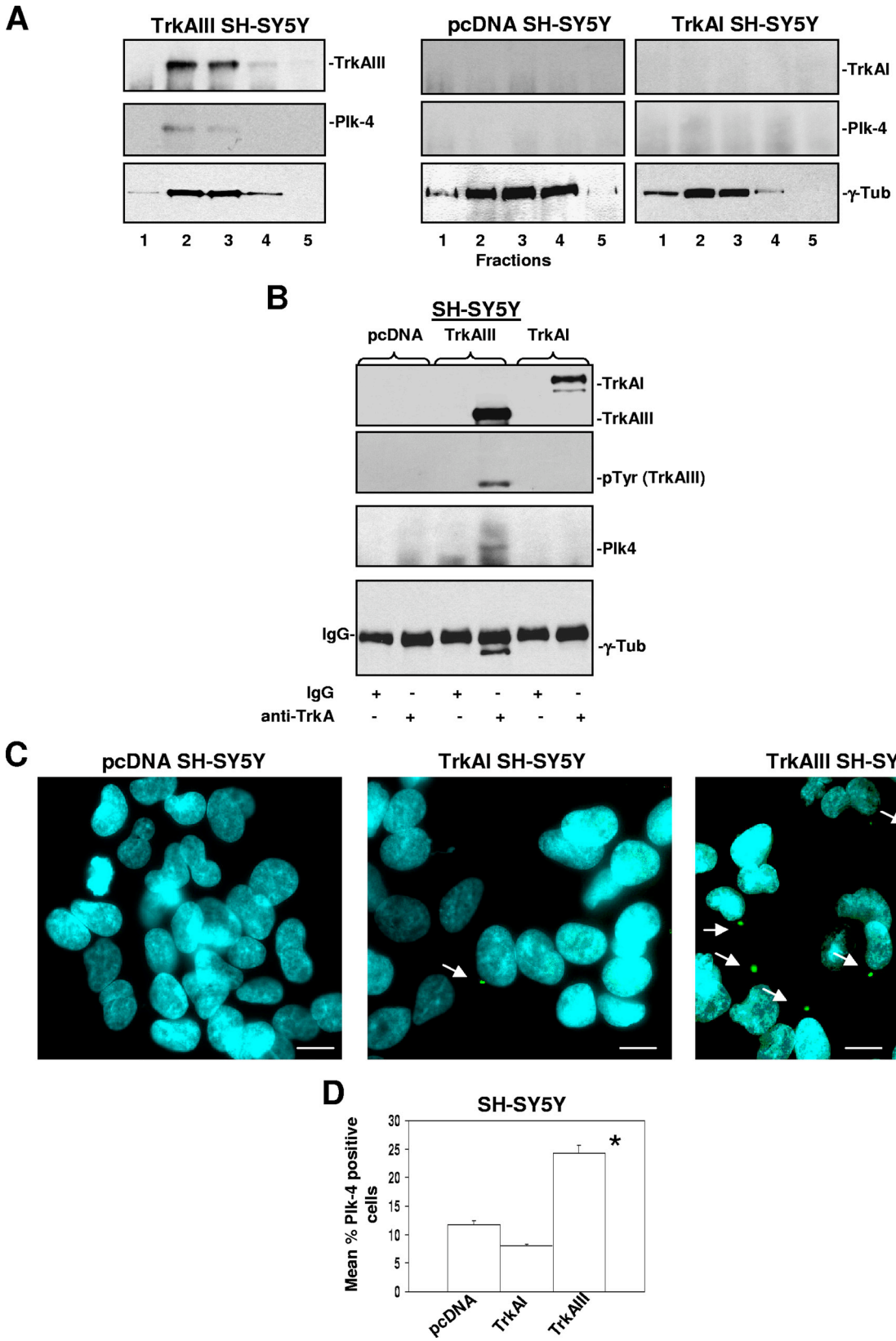


FIG. 5. TrkAIII increases Plk-4 levels at the centrosome. (A) Western blots demonstrating Plk4 and TrkAIII copurification with γ-tubulin (γ-Tub)-positive centrosomes from TrkAIII but not TrkAI or pcDNA SH-SY5Y transfectants. (B) IP/Western blots demonstrating phosphorylated-TrkAIII coimmunoprecipitation of γ-tubulin and Plk-4 from TrkAIII but not pcDNA or TrkAI transfectant extracts (preimmune IgG controls are displayed, and IgG levels in immunoprecipitates are shown as a loading control). (C) Indirect IF demonstrating high levels of perinuclear punctiform Plk-4 staining (arrows) in TrkAIII transfectants compared to the levels in pcDNA and TrkAI SH-SY5Y transfectants. Bar = 10 μm. (D) Histogram demonstrating the mean (± SD) percentages of pcDNA, TrkAI, and TrkAIII SH-SY5Y transfectants exhibiting punctiform perinuclear Plk-4 staining in six independent experiments, each representing counts from 100 individual cells (an asterisk indicates a significant statistical difference).

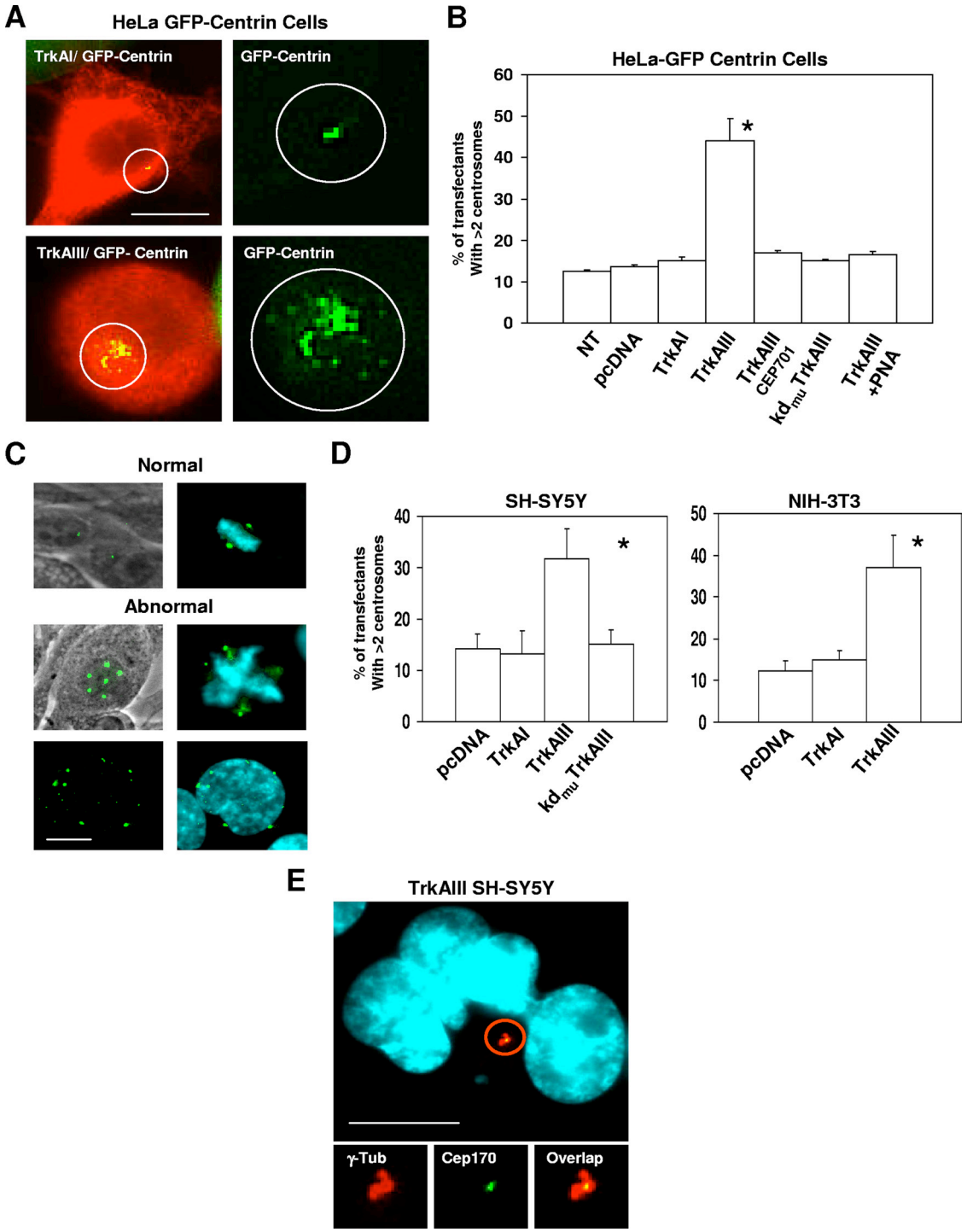


FIG. 6. TrkAIII induces centrosome amplification. (A) Indirect IF demonstrating GFP-centrin-positive centrosomes (green) in TrkAI (upper-right panel)- and TrkAIII (lower-right panel)-transfected GFP-centrin-expressing HeLa cells, plus merged (yellow) TrkAI (red; upper-left panel) or TrkAIII (red; lower-left panel), and GFP-centrin (green) expression in the same cells. Bar = 10 μm. (B) Histogram of the mean (± SD) percentages of GFP-centrin-expressing HeLa cells exhibiting centrosome amplification (>2 centrosomes per cell) following sham transfection (NT) or transient transfection with empty pcDNA vector, transient expression of TrkAI or TrkAIII, transient TrkAIII expression in the presence of 100 nM CEP-701 or 10 μM TrkAIII-PNA, or transient kd-$_{mu}$TrkAIII expression, in six independent experiments, each representing counts from 100 individual positive cells (an asterisk indicates a significant statistical difference). (C) Phase-contrast micrographs with overlapping γ-tubulin IF (green) plus Hoechst-stained chromatin (light blue) with γ-tubulin IF (green) demonstrating normal centrosome numbers and chromosome alignment in representative TrkAI SH-SY5Y transfectants (upper right and left panels, respectively) and abnormal γ-tubulin-positive centrosomes associated with aberrant chromosome alignment in representative TrkAIII SH-SY5Y transfectants (middle and lower panels). Bar = 10 μm. (D) Histograms demonstrating the mean (± SD) percentages of stable pcDNA, TrkAI, TrkAIII, and kd-$_{mu}$TrkAIII SH-SY5Y transfectants and stable pcDNA, TrkAI, and TrkAIII NIH 3T3 transfectants exhibiting >2 centrosomes per cell, in six independent experiments, each representing 100 cells per cell line (an asterisk indicates a significant statistical difference). (E) Indirect IF demonstrating centrosome amplification in a representative TrkAIII-transfected SH-SY5Y cell (bar = 10 μm), showing a merge (orange/yellow; top panel and lower-right panel) of abnormal γ-tubulin (γ-Tub)-positive centrosomes (red; lower-left panel) and a single Cep170-positive maternal centriole (green; lower-middle panel).

hibiting >2 centrosomes ($P$ values of <0.001 for TrkAIII versus both TrkAI and pcDNA transfectants and <0.02 for TrkAIII versus kd-$_{mu}$TrkAIII transfectants; Student's $t$ test). Centrosome amplification in NIH 3T3 cells was detected in 12% ± 2.4% of pcDNA transfectants and 15% ± 3.2% of TrkAI transfectants and significantly elevated to 37% ± 6.4% in TrkAIII transfectants ($P$ value of <0.001 for TrkAIII versus both pcDNA and TrkAI transfectants; Student's $t$ test) (Fig. 6D).

Centrosome amplification was confirmed in TrkAIII SH-SY5Y transfectants by indirect IF detection of frequent multiple γ-tubulin-positive centrosomes associated with a single Cep170-positive maternal centriole (Fig. 6E) (14).

**TrkAIII promotes genetic instability.** Genetic instability was assessed by evaluating abnormal mitotic spindle formation, alterations in polyploid/aneuploid status, generation of multinuclear cells, and formation of large anaplastic nuclei (11, 12).

Abnormal α-tubulin-positive mitotic spindles (Fig. 7A) were detected in 8% ± 2.6% of pcDNA SH-SY5Y transfectants, 9% ± 3.9% of TrkAI SH-SY5Y transfectants, and 12.1% ± 2.2% of kd-$_{mu}$TrkAIII transfectants, and the level was significantly elevated to 26% ± 4.3% for TrkAIII SH-SY5Y transfectants ($P$ value of <0.001 for TrkAIII versus pcDNA and TrkAI transfectants; Student's $t$ test; six experiments, each representing 100 mitotic spindle counts) (Fig. 7B). In NIH 3T3 transfectants, abnormal α-tubulin-positive mitotic spindles were detected in 10% ± 2.2% of pcDNA transfectants, 13% ± 2.6% of TrkAI transfectants, and the level was significantly elevated to 32% ± 3.6% for TrkAIII transfectants ($P < 0.001$; Student's $t$ test) (Fig. 7B).

Polyploidy, evaluated in 100 metaphase spreads per cell line and characterized by more than 100 chromosomes per cell, was detected in 3% ± 0.32% of TrkAIII SH-SY5Y transfectants but not in equivalent numbers of pcDNA, TrkAI, or kd-$_{mu}$ TrkAIII transfectants (Fig. 7C, lanes J).

Metaphase spreads confirmed a significant difference in the aneuploid status of TrkAIII SH-SY5Y transfectants, which contained a mean (± SD) of 52.2 ± 24.8 chromosomes per cell (range, 9 to 180), compared to those of pcDNA transfectants, which contained a mean of 59.7 ± 5.8 chromosomes per cell (range, 40 to 70); TrkAI transfectants, which contained a mean of 60.9 ± 5.6 chromosomes per cell (range, 53 to 74); and kd-$_{mu}$TrkAIII transfectants, which contained a mean of 60.3 ± 8.6 chromosomes per cell (range, 50 to 70) ($P$ values of <0.01 for TrkAIII versus pcDNA, TrkAI, and kd-$_{mu}$TrkAIII transfectants; Mann-Whitney/Wilcoxon rank sum test) (Fig. 7C). An increase in polyploidy and altered aneuploid status also characterized stable TrkAIII NIH 3T3 transfectants. TrkAIII NIH 3T3 transfectants contained a mean (± SD) of 98.8 ± 57.3 chromosomes per cell (range, 9 to 300), compared to pcDNA transfectants, which contained 64.1 ± 6.53 chromosomes per cell (range, 46 to 72), and TrkAI transfectants, which contained 66 ± 7.79 chromosomes per cell (range, 46 to 89) (Fig. 7D).

The generation of multinuclear cells (Fig. 7E), as an index of mitotic catastrophe, was assayed following 72 h of culture. TrkAIII SH-SY5Y transfectants generated a population of 11.2% ± 3.4% multinuclear cells, which was significantly elevated over the 2.4% ± 2.2% of multinuclear pcDNA transfectants, 2.6% ± 1.1% of multinuclear TrkAI transfectants, and 4.6% ± 0.5% of multinuclear kd-$_{mu}$TrkAIII transfectants generated over the same 72-h period (four independent experiments, each representing 100 observations; $P$ values of <0.005 for TrkAIII versus pcDNA, TrkAI, and kd-$_{mu}$TrkAIII transfectants; Student's $t$ test) (Fig. 7F). Stable TrkAIII NIH 3T3 transfectants also generated a population of 28% ± 0.4% of multinuclear cells, which represents a significantly elevation over the 5% ± 0.2% of multinuclear pcDNA and 6.3% ± 0.22% of multinuclear TrkAI NIH 3T3 transfectants generated (Fig. 7F).

Stable TrkAIII SH-SY5Y and NIH 3T3 transfectants exhibited a range of nuclear shapes and sizes, including large anaplastic nuclei, far greater than both pcDNA- and TrkAI-transfected counterparts (Fig. 7G). Stable kd-$_{mu}$TrkAIII NIH 3T3 transfectants were not available for this study.

**TrkAIII increases SCE, anaphase DNA bridging, and chromosome missegregation and alters separase interaction with the centrosome.** SCE (30 metaphase spreads per cell line; Fig. 8A) was detected in a mean (± SD) of 13.6% ± 6.8% of chromosomes per cell in TrkAIII SH-SY5Y transfectants ($n = 30$), which was significantly elevated over that detected in pcDNA (4.73% ± 2.73%), TrkAI (5.8% ± 2.04%), and kd-$_{mu}$ TrkAIII (4.2% ± 2.2%) transfectants ($P$ values of <0.001 for TrkAIII versus pcDNA, TrkAI, and kd-$_{mu}$TrkAIII transfectants; Student's $t$ test).

DNA bridging was detected in 5.6% ± 0.7% of anaphase TrkAIII SH-SY5Y transfectants, which is significantly higher than the corresponding percentages of pcDNA (0.5% ± 0.3%), TrkAI (1.5% ± 0.8%), and kd-$_{mu}$TrkAIII (2.3% ± 0.3%) transfectants (Fig. 8B). Complete chromosome missegregation (Fig. 8C) was detected in 3.6% ± 0.5% of TrkAIII SH-SY5Y transfectants but not in equivalent numbers of pcDNA, TrkAI, or kd-$_{mu}$TrkAIII transfectants (four experiments, each representing 100 observations) (Fig. 8D).

Indirect IF detected normal patterns of separase-centrosome interaction during prometaphase through late metaphase but not anaphase through telophase (Fig. 8E) in relatively more pcDNA and TrkAI transfectants than TrkAIII SH-SY5Y transfectants (Fig. 8E and F). Lack of separase-centrosome interaction (Fig. 8F) was detected in 67.9% ± 9.9% of metaphase TrkAIII SH-SY5Y transfectants, compared to 25.4% ± 6.4% of pcDNA-transfected counterparts, 24.7% ± 9.1% of TrkAI-transfected counterparts, and 25.3% ± 4.6% of kd-$_{mu}$TrkAIII-transfected counterparts (four experiments, each representing 100 observations per cell line; $P$ values of <0.001 for TrkAIII versus pcDNA, TrkAI, and kd-$_{mu}$TrkAIII; Student's $t$ test) (Fig. 8G). These data suggest that TrkAIII impedes separase interaction and function at the centrosome.

**TrkAIII-PNA.** TrkAIII–PNA–D-$(AAKK)_4$ conjugate (10 μM) inhibited TrkAIII but not TrkAI protein expression in respective SH-SY5Y transfectants following 14-day treatment, as detected by Western blotting (Fig. 9A) and indirect IF (Fig. 9C, upper panels). In [3-(4,5-dimethylthiazol-2yl)-5(3-carboxymethonyphenol)-2-(4-sulfophenyl)-2H-tetrazolium] (MTS) proliferation assays, TrkAIII transfectants but not pcDNA or stable TrkAI SH-SY5Y transfectants treated for 14 days with 10 μM TrkAIII-PNA exhibited a significant 20.8% reduction ($P < 0.05$; Student's $t$ test) in proliferation (Fig. 9B). TrkAIII-PNA also reversed the highly lobular anaplastic nuclear phenotype exhibited by TrkAIII but not TrkAI SH-SY5Y transfectants (Fig. 9C). These data confirm TrkAIII-PNA as a

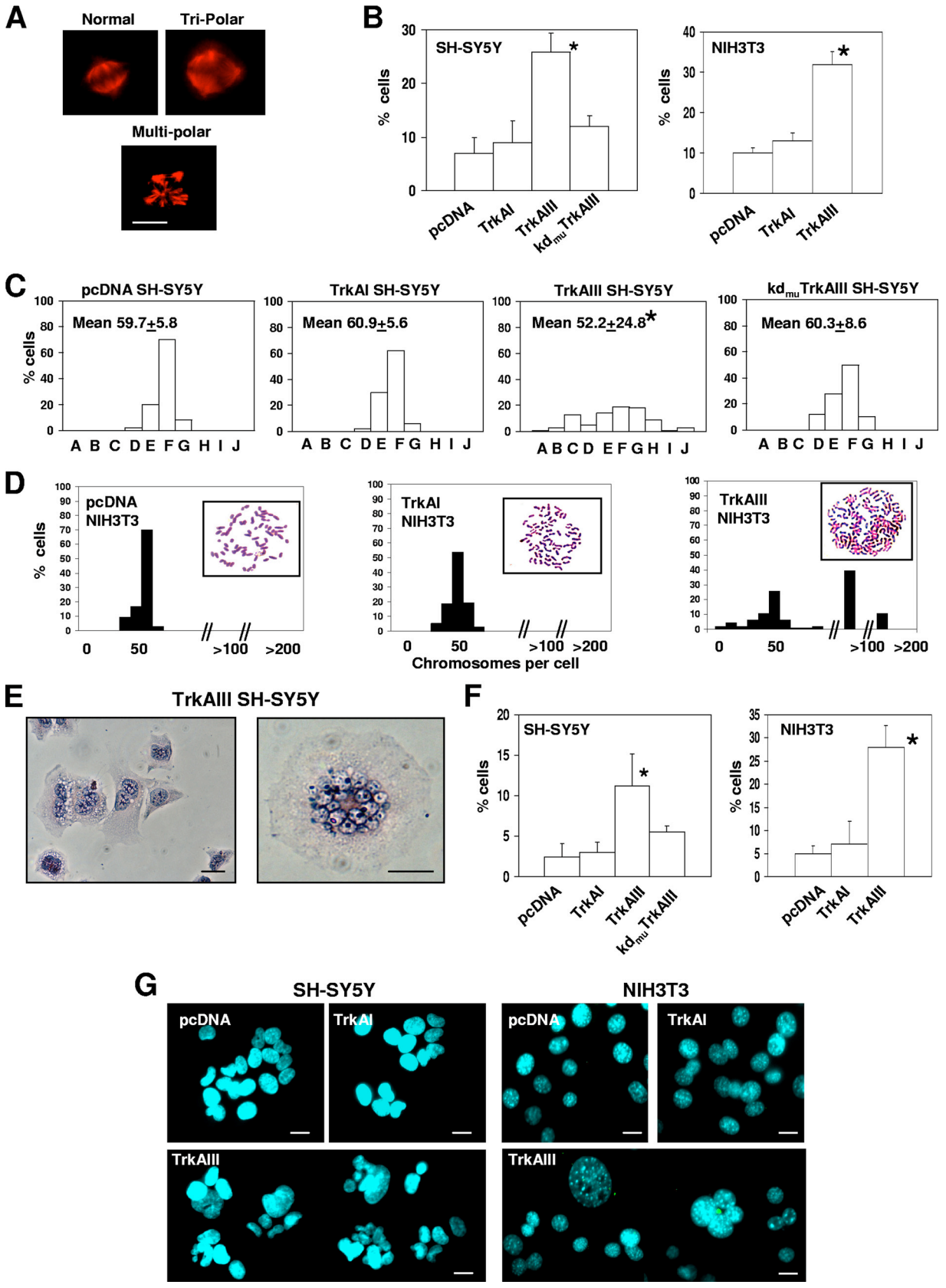


FIG. 7. TrkAIII promotes genetic instability in SH-SY5Y cells. Asterisks indicate significant statistical differences. (A) Indirect IF demonstrating α-tubulin-positive (red) normal, tripolar, and multipolar mitotic spindles in SH-SY5Y transfectants. Bar = 10 μm. (B) Histograms demonstrating the mean (± SD) percentages of mitotic pcDNA, TrkAI, TrkAIII, and kd-$_{mu}$TrkAIII SH-SY5Y transfectants and mitotic pcDNA,

specific inhibitor of TrkAIII expression and implicate TrkAIII in regulating proliferation and anaplastic nuclear morphology in SH-SY5Y cells.

## DISCUSSION

We report an important novel function for the alternative TrkAIII splice variant as an inducer of centrosome amplification and promoter of genetic instability. This function depends upon the intracellular TrkAIII retention, accumulation, and spontaneous interphase-restricted activation, in a cytoplasmic tk domain orientation, within membranes that closely associate with the fully assembled ER/ERGIC/GN compartment. TrkAIII activated within this novel membrane-substrate context is regulated by endogenous PTPase activity, GA-sensitive interaction with Hsp90, and ERGIC/GN assembly status and acquires the capacity to bind γ-tubulin, resulting in recruitment to the centrosome. This causes differential phosphorylation of several centrosome-associated components, increases centrosome interaction with Plk-4, and decreases centrosome interaction with separase, leading to centrosome amplification and increased genetic instability.

The spontaneous activation of intracellular TrkAIII detected in stably transfected SH-SY5Y and NIH 3T3 cell lines (44), combined with TrkAIII function in human HeLa cells and endogenous TrkAIII-associated tyrosine phosphorylation in human neural U251 glioma cells, confirms that TrkAIII activation is not cell type or clone specific or confined to conditions of overexpression. However, since alternative TrkAIII splicing is stress regulated in NB cells (44), TrkAIII activity is regulated by endogenous PTPases and interaction with Hsp90 (this study), and the outcome of TrkAIII-induced centrosome amplification is likely to depend upon oncosuppressor status (6, 7, 35, 40, 42, 49, 53), the effect of TrkAIII expression upon cell behavior is likely to exhibit some degree of cell specificity.

TrkAIII intracellular accumulation, caused by exon 6 and 7 skipping and associated with complete impediment of cell surface translocation (unpublished data), is likely to depend upon the omission of N-glycosylation sites within exons 6 and 7, which have been implicated in TrkA cell surface expression (44, 48), and is consistent with reports that reduced N-glycosylation promotes receptor tk intracellular entrapment (5, 13, 46).

The high-level ER retention exhibited by TrkAIII indicates difficulty in overcoming ER quality control, supported by alternative folding and constitutive binding of calnexin and Grp78/BiP exhibited by ER-associated TrkAIII. TrkAIII also accumulates within non-ER membranes in association with the loss of alternative folding and calnexin and Grp78/BiP binding, indicating eventual ER quality control satisfaction. TrkAIII SH-SY5Y transfectants, however, do not exhibit constitutive alternative splicing of the ER stress response transcription factor XBP-1, indicating that TrkAIII ER perturbation is below the threshold for activation of the Ire1α branch of the ER stress response (51).

TrkAIII tyrosine phosphorylation, detected in ER and non-ER membranes, was localized by indirect IF primarily to perinuclear vesicle-like structures at the center of the calnexin-positive ER that closely associate with and overlap GM130, TGN46, and, in particular, ERGIC-53 expression, suggesting relative restriction to structures associated with the assembled ERGIC/GN. This was supported using the ERGIC/GN-disrupting agent BFA (43), which abrogated TrkAIII tyrosine phosphorylation. The observation that TrkAIII-associated tyrosine phosphorylation does not occur throughout the calnexin-positive ER may not only depend upon alternative TrkAIII folding and TrkAIII binding of GRP78/BiP, which inactivates ER-associated receptor tks (20), but also endogenous ER-associated PTPase activity (10), as suggested by sodium orthovanadate stimulation of TrkAIII tyrosine phosphorylation. The localization of TrkAIII-associated tyrosine phosphorylation to the center of the calnexin-positive ER suggests that conditions favorable for TrkAIII activity within the ER lie adjacent to the ERGIC/GN, which would include both ER exit sites and anterograde COP II transport vesicles (1).

The possibility that TrkAIII-associated tyrosine phosphorylation represents an artifact of overexpression is diminished by the observations that significant intracellular TrkAI accumulation within the GN and that similar intracellular levels of kd-$_{mu}$TrkAIII did not associate with tyrosine phosphorylation and by endogenous TrkAIII-associated tyrosine phosphorylation in human neural U251 glioma cells. U251 cells were chosen to study endogenous TrkAIII, as they exhibit constitutive predominant endogenous TrkAIII expression under normal conditions. This is in contrast to NB cells that exhibit stress-induced and not constitutive endogenous TrkAIII expression (44, 45; this study), which complicates the study of endogenous TrkAIII behavior due to the collateral effects associated with cellular stress. Intracellular endogenous TrkAIII expression by U251 cells was inhibited by TrkAIII-PNA, confirming its identity, and was associated with intracellular tyrosine phosphorylation, which was inhibited by the pan-Trk tk inhibitor CEP-701 (4). This indicates that TrkAIII-associated tyrosine phosphorylation is not restricted to conditions of overexpression and sustains our

TrkAI, and TrkAIII NIH 3T3 transfectants exhibiting abnormal (tripolar, multipolar, and pseudobipolar) spindles in six independent experiments, each representing 100 individual cells. (C) Histograms of the percentages of pcDNA, TrkAI, TrkAIII, and kd-$_{mu}$TrkAIII SH-SY5Y transfectants containing 1 to 9 (column A), 10 to 19 (column B), 20 to 29 (column C), 30 to 39 (column D), 40 to 49 (column E), 50 to 59 (column F), 60 to 69 (column G), 70 to 79 (column H), 80 to 89 (column I), and >100 (column J) chromosomes in 100 metaphase spreads for each cell line, plus mean (± SD) chromosome numbers per cell line. (D) Histograms, containing representative metaphase chromosome spreads (inserts), demonstrating chromosome number distribution in 100 metaphase spreads in pcDNA, TrkAI, and TrkAIII NIH 3T3 transfectants. (E) Light micrographs of polynuclear TrkAIII SH-SY5Y transfectants. Bar = 10 μm. (F) Histograms demonstrating the mean (± SD) percentages of multinuclear cells (≥2 nuclei per cell) generated following 72-h culture of equal numbers of pcDNA, TrkAI, TrkAIII, and kd-$_{mu}$TrkAIII SH-SY5Y transfectants and pcDNA, TrkAI, and TrkAIII NIH 3T3 transfectants in six independent experiments, each representing 100 individual cells. (G) Representative Hoechst fluorescence demonstration of typical nuclear shapes and sizes exhibited by pcDNA-, TrkAI-, and TrkAIII-transfected SH-SY5Y cells and pcDNA, TrkAI, and TrkAIII NIH 3T3 transfectants. Bar = 10 μm.

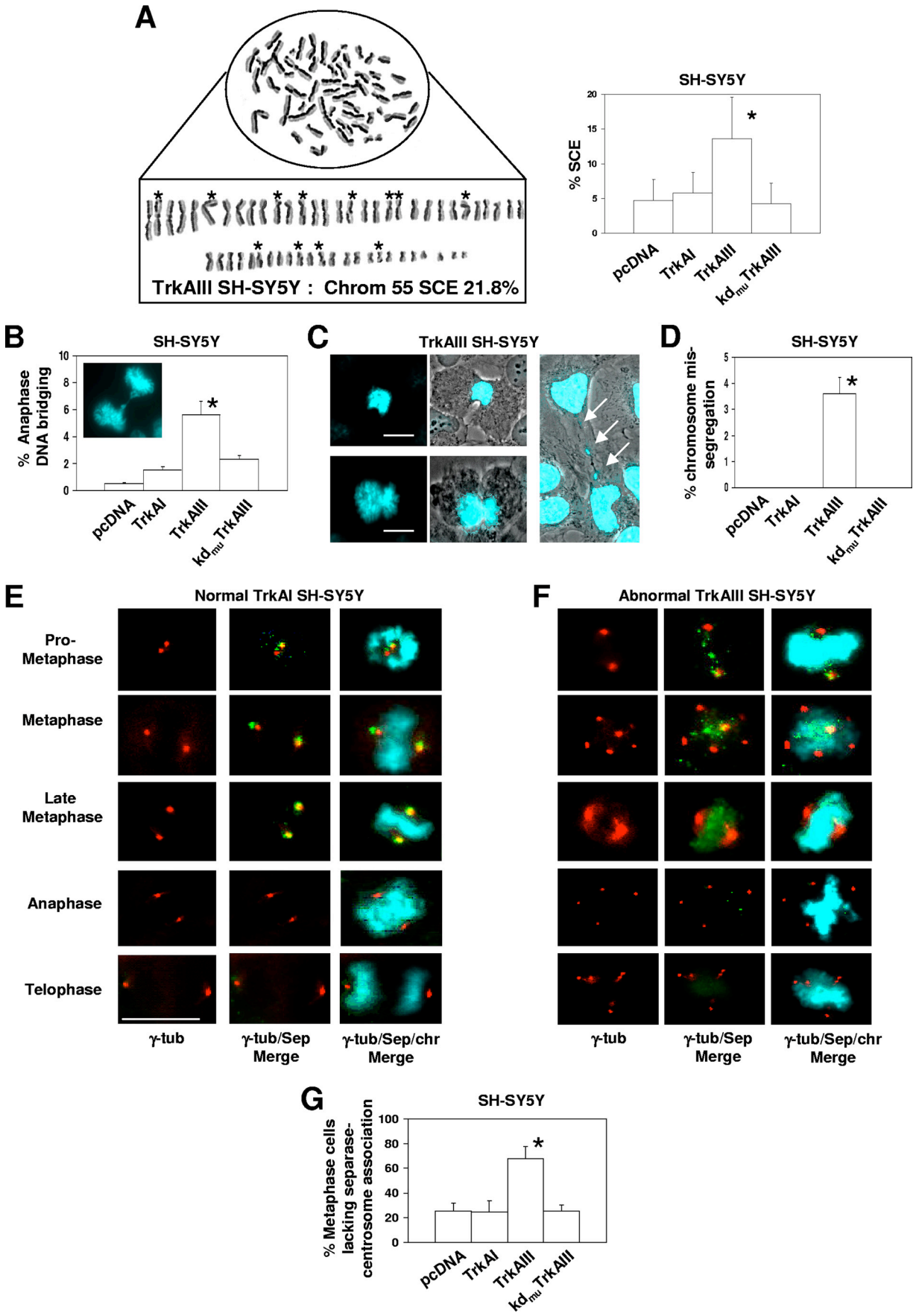

hypothesis that constitutive TrkAIII activation results primarily from intracellular entrapment caused by reduced extracellular domain N glycosylation (48) and subsequent ligand-independent activation facilitated by omission of the extracellular Ig $C_1$ domain within alternatively spliced exons 6 and 7 (2).

TrkAIII-associated tyrosine phosphorylation was detected during interphase, inhibited during mitosis, and reactivated postcytokinesis, confirming cell cycle regulation. This is likely to depend upon cell cycle-regulated PTPases (10, 32), supported by sodium orthovanadate stimulation of TrkAIII tyrosine phosphorylation and also upon cycles of ERGIC/GN disruption and reassembly (15), supported by BFA (43) inhibition of TrkAIII tyrosine phosphorylation. Furthermore, inhibitor studies demonstrating CEP-701 and BFA inhibition of TrkAIII tyrosine phosphorylation and sodium orthovanadate stimulation of TrkAIII tyrosine phosphorylation but no effect of NGF-neutralizing antibody, A2a adenosine receptor antagonist, and c-Src inhibitor indicate that TrkAIII activation differs from both ligand-dependent activation of mature cell surface TrkA (TrkAI/TrkAII) and A2a adenosine receptor/c-Src-mediated activation of immature GN-associated TrkA (TrkAI/TrkAII) (37) in being spontaneous, ligand independent, Trk tk mediated, and dependent upon full ER/ERGIC/GN assembly.

A cytoplasmic orientation for the active TrkAIII tk domain within internal ER/ERGIC/GN membranes, confirmed by chymotrypsin digestion as described for GN-associated GM130 but not mannosidase II (52), would place TrkAIII activity in close proximity to the centrosome (38). Indeed, TrkAIII interaction with the centrosome was confirmed by the observations that (i) TrkAIII but not TrkAI- or kd-$_{mu}$TrkAIII-bound γ-tubulin, (ii) tyrosine-phosphorylated TrkAIII but not TrkAI or kd-$_{mu}$TrkAIII copurified with γ-tubulin-positive centrosomes, and (iii) γ-tubulin coimmunoprecipitated TrkAIII from purified centrosome preparations. TrkAIII tk involvement in this interaction, suggested by the lack of γ-tubulin binding exhibited by nonphosphorylated TrkAI and kd-$_{mu}$TrkAIII, was supported by CEP-701 inhibition of TrkAIII tyrosine phosphorylation and γ-tubulin binding and by sodium orthovanadate stimulation of TrkAIII tyrosine phosphorylation and γ-tubulin binding. The requirement for full ERGIC/GN assembly for this interaction was also supported by BFA inhibition of TrkAIII tyrosine phosphorylation and γ-tubulin binding, and a role for Hsp90 was suggested by GA (33) inhibition of TrkAIII tyrosine phosphorylation and γ-tubulin binding. These data indicate that TrkAIII exhibits a unique binding interaction with γ-tubulin, dependent upon druggable PTPase-regulated and Hsp90-dependent TrkAIII tk activity within the context of full ER/ERGIC/GN assembly.

TrkAIII tk function at the centrosome was confirmed by the differential tyrosine phosphorylation of several centrosome-associated components in TrkAIII SH-SY5Y transfectants compared to TrkAI SH-SY5Y transfectants and was reversed by the pan-Trk inhibitor CEP-701 (4). This indicates that TrkAIII alters the kinase/phosphate equilibrium at the centrosome. Of these differentially phosphorylated components, the 100-kDa protein is likely to represent TrkAIII, whereas the remaining 70-kDa, 60-kDa, 48-kDa, 38-kDa, and 33-kDa components remain to be identified. Consistent with TrkAIII tk function at the centrosome, transient TrkAIII expression in GFP-centrin-expressing HeLa cells deregulated centrosome duplication, resulting in centrosome amplification (34). This effect was not observed following transient pcDNA, TrkAI, or kd-$_{mu}$TrkAIII transfection and was inhibited by CEP-701 and TrkAIII-PNA, confirming dependence upon TrkAIII expression and TrkAIII tk activity. Increased levels of centrosome amplification, confirmed by the presence of multiple centrosomes containing a single Cep170-positive maternal centriole (14), also characterized TrkAIII SH-SY5Y and NIH 3T3 stable transfectants but not pcDNA- and TrkAI-transfected counterparts, further confirming that TrkAIII promotes centrosome amplification. Potential mechanisms through which TrkAIII promotes centrosome amplification in addition to altering the kinase/phosphate equilibrium that tightly regulates centrosome duplication (27) include TrkAIII promotion of Plk-4 interaction with the centrosome, reported to induce rapid centrosome amplification (18), and TrkAIII impairment of separase interaction with the centrosome, also reported to result in centrosome amplification (41, 47).

Increased genetic instability associated with centrosome amplification, characterized by increased abnormal mitotic spindle formation, altered polyploid/aneuploid status, increased generation of multinuclear cells, and a wide range of nuclear shapes and sizes, including large anaplastic nuclei (11, 12), was detected in TrkAIII transfectants but not pcDNA, TrkAI, or



FIG. 8. TrkAIII reduces separase interaction at the centrosome. (A) Representative SCE assay demonstrating SCE in a TrkAIII SH-SY5Y transfectant (circled panel), with aligned chromosomes, chromosome numbers (Chrom), and SCE percentage presented (boxed panel), plus a histogram demonstrating the mean (± SD) percentage of SCE in 30 metaphase spreads per pcDNA, TrkAI, TrkAIII, and kd-$_{mu}$TrkAIII SH-SY5Y cell lines (an asterisk indicates a significant statistical difference). (B) Fluorescence micrograph (insert) demonstrating anaphase DNA bridging in a representative TrkAIII SH-SY5Y transfectant plus a histogram of the mean (± SD) percentages of pcDNA, TrkAI, TrkAIII, and kd-$_{mu}$TrkAIII SH-SY5Y transfectants exhibiting anaphase DNA bridging (six independent experiments, each representing 100 observations per cell line). (C) Phase-contrast and overlapping fluorescence micrographs demonstrating chromosome missegregation in representative TrkAIII SH-SY5Y transfectants (bar = 10 μm) plus evidence of continuous DNA strands with micronuclei (arrows) linking two TrkAIII SH-SY5Y transfectants postcytokinesis. (D) Histogram demonstrating the mean (± SD) percentages of mitotic pcDNA, TrkAI, TrkAIII, and kd-$_{mu}$TrkAIII SH-SY5Y transfectants exhibiting chromosome missegregation in six independent experiments, each representing 100 observations per cell line. (E) Indirect IF demonstrating normal γ-tubulin (γ-tub) (red; left panels), merged γ-tubulin (red)/separase (Sep) (green) expression (middle panels) plus Hoechst stained chromatin (chr) (light blue; right panels) in representative prometaphase-through-telophase TrkAI SH-SY5Y transfectants. (F) Indirect IF demonstrating abnormal γ-tubulin expression (red; left panels), merged γ-tubulin (red)/separase (green) expression (middle panels), and Hoechst-stained chromatin (light blue; right panels) in representative mitotic TrkAIII SH-SY5Y transfectants. Bar = 10 μm. (G) Histogram of the mean (± SD) percentages of pcDNA, TrkAI, TrkAIII and kd-$_{mu}$TrkAIII SH-SY5Y transfectants exhibiting a lack of separase/γ-tubulin association during metaphase in six independent experiments, each representing 100 observations per cell line (an asterisk indicates a significant statistical difference).

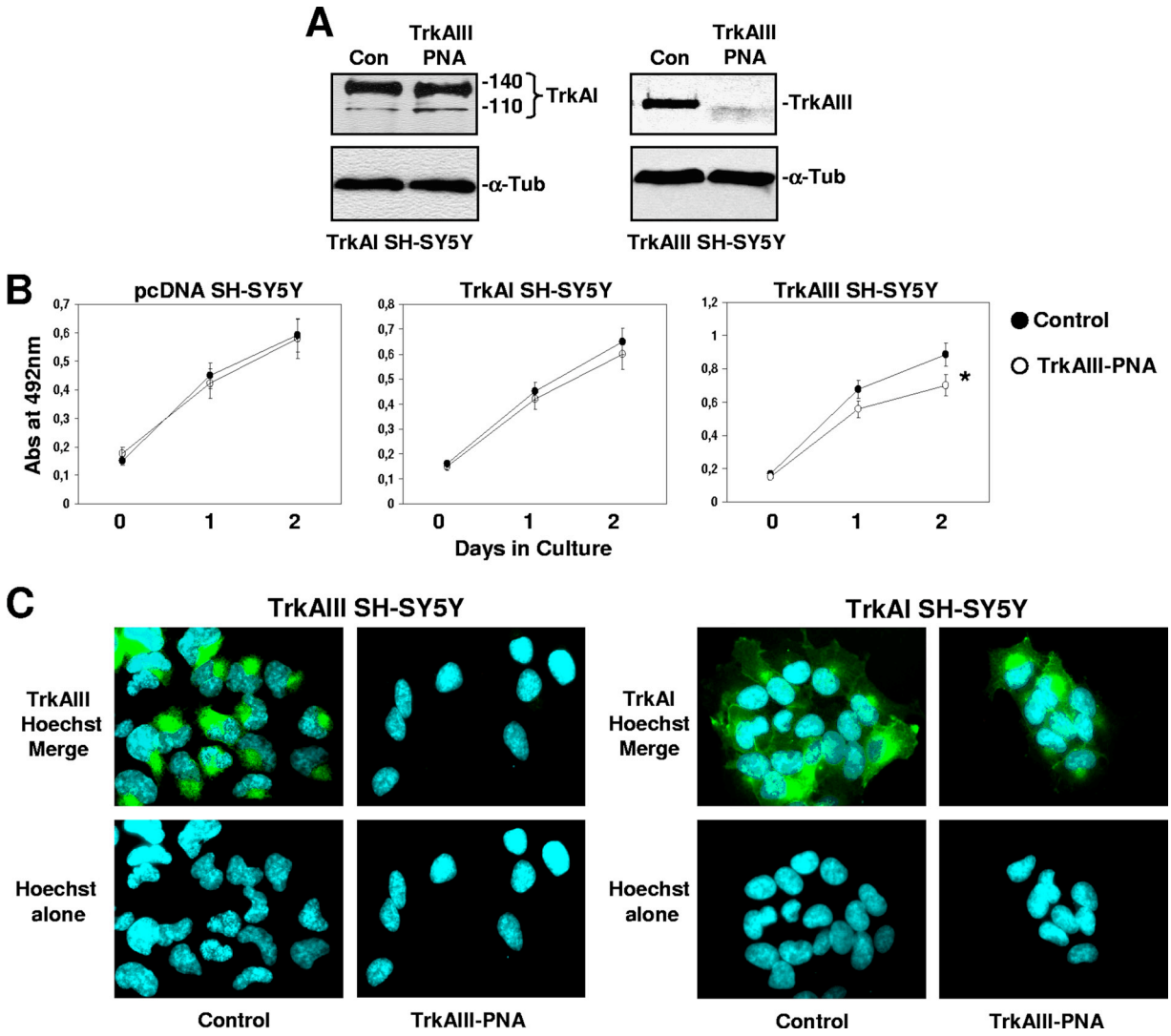


FIG. 9. PNA knockdown of TrkAIII expression. (A) Western blots demonstrating inhibition of TrkAIII but not TrkAI or α-tubulin (α-Tub) expression in TrkAIII and TrkAI SH-SY5Y transfectants (Con) treated for 14 days with 10 μM TrkAIII-PNA. (B) Line graphs demonstrating significant inhibition (*) of TrkAIII but not pcDNA or TrkAI SH-SY5Y transfectant proliferation in 2-day MTS proliferation assays initiated 14 days following treatment with or without (control) 10 μM TrkAIII PNA (mean ± SD MTS reagent absorbance [Abs] at 492 nm, in duplicate experiments performed using six cultures per cell line per time point). (C) Indirect IF demonstrating the inhibitory effect of 14-day treatment with 10 μM TrkAIII-PNA upon TrkAIII (green; upper-left two panels, control versus TrkAIII-PNA) but not TrkAI (green; upper-right two panels, control versus TrkAIII-PNA) expression plus the effect of 14-day treatment with 10 μM TrkAIII-PNA upon Hoechst-stained lobular nuclear morphology in TrkAIII (blue; lower-left two panels, control versus TrkAIII-PNA) but not TrkAI (lower-right two panels, control versus TrkAIII-PNA) SH-SY5Y transfectants.

kd-$_{mu}$TrkAIII transfectants, confirming dependence upon TrkAIII expression and TrkAIII tk activity. TrkAIII transfectants but not pcDNA, TrkAI, or kd-$_{mu}$TrkAIII transfectants also exhibited increased chromosome missegregation and anaphase DNA bridging, associated with impaired centrosome association with separase, reported to result in similar manifestations (41, 47), and exhibited increased levels of SCE, suggesting elevated levels of homologous recombination and/or an elevated burden of single-strand DNA breaks similar to that reported for JAK2 oncogenic tk (36).

TrkAIII promotion of centrosome amplification and genetic instability is associated with more malignant behavior, characterized by TrkAIII induction of NIH 3T3 tumorigenic activity and promotion of SH-SY5Y primary and metastatic xenograft tumorigenic activity (44, 45). It should be noted, however, that centrosome amplification in normal cells may act as a backup to the mitotic spindle checkpoint, promoting mitotic catastrophe and oncosuppressor-mediated senescence and/or apoptosis (21, 53). This suggests that tumor suppressor inactivation may be a prerequisite for the oncogenic effect of TrkAIII detected in SH-SY5Y and NIH 3T3 cells. This is supported by reports that link p53, adenomatous polyposis coli gene, and ATM inactivation to centrosome amplification and subsequent oncogenesis (7, 40, 49), and these results sustain the association between centrosome amplification and tumor malignancy and support the hypothesis that centrosome amplification

represents a fundamental oncogenic mechanism (11, 12, 26, 35, 49).

In support of our hypothesis that TrkAIII represents an important and potentially druggable target in NB, we identified the pan-Trk inhibitor CEP-701 (4) as an inhibitor of TrkAIII tk activity, TrkAIII binding of γ-tubulin, and TrkAIII induction of centrosome amplification; the ERGIC/GN-disrupting agent BFA (43) and the Hsp90 inhibitor GA (33) as inhibitors of TrkAIII tk activity and binding of γ-tubulin; and a novel TrkAIII-PNA as a specific inhibitor of TrkAIII expression, TrkAIII-induced centrosome amplification, TrkAIII transfectant proliferation, and TrkAIII-induced anaplastic lobular nuclear morphology. We are currently developing novel TrkAIII-PNA formulations to optimize uptake and targeting and reduce inhibitory concentrations for future use, in combination with inhibitors of TrkAIII tk activity in NB models in vivo.

In conclusion, we characterize TrkAIII as a novel and rare example of an intracellular membrane-associated oncogenic tk that targets the centrosome, induces centrosome amplification, and promotes genetic instability. We propose that this novel function, facilitated by spontaneous ligand-independent activation within the context of a fully assembled ER/ERGIC/GN compartment, results in acquisition of γ-tubulin-binding activity and TrkAIII recruitment to the centrosome. This in turn alters the kinase/phosphate equilibrium at the centrosome and increases Plk-4 but reduces separase interaction with the centrosome, leading to centrosome amplification and promotion of genetic instability. This unveils an important and novel alternative mechanism to "classical" cell surface oncogenic receptor tk signaling (3), through which TrkAIII and potentially other oncogenic tk receptors that localized in an active form to intracellular membranes (13, 50) exert oncogenic activity.

## ACKNOWLEDGMENTS

We thank G. Guarguaglini (Rome University La Sapienza) for the anti-Cep-170 antibody and B. Cinque, N. Di Ianni, and M. Zani and postgraduate students Paolo Ciufici, Stefania Merolle, and Marzia Ragone for technical assistance.

This work was supported by grants from AIRC, Telethon GGP07118, Progetto Speciale Ministero Della Sanità, MURST-Cofin, the MIUR-CNR-Oncology project, and the Centre of Excellence BEMM and Rome Oncogenomic Center.

This work is dedicated to the students of L'Aquila University who lost their lives in the earthquake on the 6 April 2009.

## REFERENCES

1. **Appenzeller-Herzog, C., and H.-P. Hauri.** 2006. The ER-Golgi intermediate compartment (ERGIC): in search of its identity and function. J. Cell Sci. **119:**2173–2183.
2. **Arevalo, J. C., B. Conde, B. L. Hempstead, M. V. Chao, D. Martin-Zanca, and P. Perez.** 2000. TrkA immunoglobulin-like ligand binding domains inhibit spontaneous activation of the receptor. Mol. Cell. Biol. **20:**5908–5916.
3. **Blume-Jensen, P., and T. Hunter.** 2001. Oncogenic kinase signalling. Nature **411:**355–365.
4. **Camoratto, A. M., J. P. Jani, T. S. Angeles, A. C. Maroney, C. Y. Sanders, C. Murakata, N. T. Neff, J. L. Vaught, J. T. Isaacs, and C. A. Dionne.** 1997. CEP-751 inhibits Trk receptor tyrosine kinase activity in vitro and exhibits anti-tumor activity. Int. J. Cancer **72:**673–679.
5. **Collier, E., J. L. Carpentier, L. Beitz, H. Caro, S. I. Taylor, and P. Gorden.** 1993. Specific glycosylation site mutations of insulin receptor alpha subunit impairs intracellular transport. Biochemistry **32:**7818–7823.
6. **Delaval, B., S. Létard, H. Lelièvre, V. Chevrier, L. Daviet, P. Dubreuil, and D. Birnbaum.** 2005. Oncogenic tyrosine kinase of malignant hemopathy targets the centrosome. Cancer Res. **65:**7231–7240.
7. **Dikovskaya, D., D. Schiffmann, I. P. Newton, A. Oakley, K. Kroboth, O. Sansom, T. J. Jamieson, V. Meniel, A. Clarke, and I. S. Nathke.** 2007. Loss of APC induces polyploidy as a result of a combination of defects in mitosis and apoptosis. J. Cell Biol. **176:**183–195.
8. **Dionisotti, S., E. Ongini, C. Zocchi, B. Kull, G. Arslan, and B. B. Fredholm.** 1997. Characterisation of human $A_{2A}$ adenosine receptors with the antagonist radioligand [$^3$H]-SCH 58261. Br. J. Pharmacol. **121:**353–360.
9. **Eggert, A., M. A. Grotzer, N. Ikegaki, X. G. Liu, A. E. Evans, and G. M. Brodeur.** 2002. Expression of the neurotrophin receptor TrkA down-regulates expression and function of angiogenic stimulators in SH-SY5Y neuroblastoma cells. Cancer Res. **62:**1802–1808.
10. **Frangioni, J. V., P. H. Beahm, V. Shifrin, C. A. Jost, and B. G. Neel.** 1992. The non transmembrane tyrosine phosphatase PTP-1B localises to the endoplasmic reticulum via its 35 amino acid C-terminal sequence. Cell **68:**545–560.
11. **Fukasawa, K.** 2005. Centrosome amplification, chromosome instability and cancer development. Cancer Lett. **230:**6–19.
12. **Fukasawa, K.** 2007. Oncogenes and tumour suppressors take on the centrosome. Nat. Rev. Cancer **7:**911–924.
13. **Gibbs, L., and L. Legeai-Mallet.** 2007. FGFR3 intracellular mutations induce tyrosine phosphorylation in the Golgi and defective glycosylation. Biochim. Biophys. Acta **1773:**502–512.
14. **Guarguaglini, G., P. I. Duncan, Y. D. Stierhof, T. Holmstrom, S. Duensing, and E. A. Nigg.** 2005. The forkhead-associated domain protein Cep170 interacts with Polo-like kinase 1 and serves as a marker for mature centrioles. Mol. Biol. Cell **16:**1095–1107.
15. **Jesch, S. A., and A. D. Linstedt.** 1998. The Golgi and endoplasmic reticulum remain independent during mitosis in HeLa cells. Mol. Biol. Cell **9:**623–635.
16. **Kaihatsu, K., K. E. Huffman, and D. A. Corey.** 2004. Intracellular uptake and inhibition of gene expression by PNAs and PNA-peptide conjugates. Biochemistry **43:**14340–14347.
17. **Kalnina, Z., P. Zayakin, K. Silina, and A. Line.** 2005. Alterations of pre-mRNA splicing in cancer. Genes Chromosomes Cancer **42:**342–357.
18. **Kleylein-Sohn, J., J. Westerndorf, M. Le Clech, R. Habedank, Y. D. Stierhof, and E. A. Nigg.** 2007. Plk-4 induced centriole biogenesis in human cells. Dev. Cell **13:**190–202.
19. **Lavenius, E., C. Gestblom, I. Johansson, E. Nanberg, and S. Pahlman.** 1995. Transfection of Trk-A into human neuroblastoma cells restores their ability to differentiate in response to nerve growth factor. Cell Growth Differ. **6:**727–736.
20. **Liu, G., Y. Shang, and Y. Yu.** 2006. Induced endoplasmic reticulum (ER) stress and binding of over-expressed ER specific chaperone GRP78/BIP with dimerized epidermal growth factor receptor in mammalian cells exposed to low concentration of N′-methyl-N-nitro-N-nitrosoguanidine. Mutat. Res. **596:**12–21.
21. **Löffler, H., J. Lukas, J. Bartek, and A. Kramer.** 2006. Structure meets function-centrosomes, genome maintenance and the DNA damage response. Exp. Cell Res. **312:**2633–2640.
22. **Lucarelli, E., D. Kaplan, and C. J. Thiele.** 1997. Activation of trk-A but not trk-B signal transduction pathway inhibits growth of neuroblastoma cells. Eur. J. Cancer **33:**2068–2070.
23. **Lüders, J., and T. Stearns.** 2007. Microtubule organising centres: a re-evaluation. Nat. Rev. Mol. Cell Biol. **8:**161–167.
24. **Lüders, J., U. K. Patel, and T. Stearns.** 2006. GCP-WD is a gamma tubulin targeting factor required for centrosomal and chromatin mediated microtubule nucleation. Nat. Cell Biol. **8:**137–147.
25. **Meakin, S. O., and E. M. Shooter.** 1991. Tyrosine kinase activity coupled to the high-affinity nerve growth factor-receptor complex. Proc. Natl. Acad. Sci. USA **88:**5862–5866.
26. **Meijer, G. A.** 2005. Chromosomes and cancer. Boveri revisited. Cell. Oncol. **27:**273–275.
27. **Meraldi, P., and E. A. Nigg.** 2001. Centrosome cohesion is regulated by a balance of kinase and phosphatase activities. J. Cell Sci. **114:**3749–3757.
28. **Missbach, M., E. Altmann, L. Widler, M. Susa, E. Buchdunger, H. Mett, T. Meyer, and J. Green.** 2000. Substituted 5, 7-diphenyl-pyrrolo [2,3*d*] pyrimidines: potent inhibitors of the tyrosine kinase c-Src. Bioorg. Med. Chem. Lett. **10:**945–949.
29. **Modrek, B., and C. Lee.** 2002. A genomic view of alternative splicing. Nat. Genet. **30:**13–19.
30. **Nakagawara, A.** 2001. Trk receptor tyrosine kinases: a bridge between cancer and neural development. Cancer Lett. **169:**107–114.
31. **Nigg, E. A.** 2007. Centrosome duplication: of rules and licenses. Trends Cell Biol. **17:**215–221.
32. **Noll, A., S. L. Ruppenthal, and M. Montenarh.** 2006. The mitotic phosphatase cdc25C at the Golgi apparatus. Biochem. Biophys. Res. Commun. **351:**825–830.
33. **Onuoha, S. C., S. R. Mukund, E. T. Coulstock, B. Sengerova, J. Shaw, S. H. Mclaughlin, and S. E. Jackson.** 2007. Mechanistic studies on Hsp90 inhibition by ansamycin derivatives. J. Mol. Biol. **372:**287–297.
34. **Piel, M., P. Meyer, A. Khodjakov, C. L. Reider, and M. Bornens.** 2000. The respective contributions of the mother and daughter centrioles to centrosome activity and behaviour in vertebrate cells. J. Cell Biol. **149:**317–330.
35. **Pihan, G. A., A. Purohit, J. Wallace, H. Knecht, B. Woda, P. Queensberry, and S. J. Doxsey.** 1998. Centrosome defects and genetic instability in malignant tumors. Cancer Res. **58:**3974–3985.
36. **Plo, I., M. Nakatake, L. Malivert, J. P. de Villartay, S. Giraudier, J. L.**

**Villeval, L. Wiesmuller, and W. Vainchenker.** 2008. JAK2 stimulates homologous recombination and genetic instability: potential implication in the heterogeneity of myeloproliferative disorders. Blood **122:**1402–1412.
37. **Rajagopal, R., Z. Y. Chen, F. S. Lee, and M. V. Chao.** 2004. Transactivation of Trk neurotrophin receptors by G-protein coupled receptor ligands occurs on intracellular membranes. J. Neurosci. **24:**6650–6658.
38. **Rios, R. M., and M. Bornens.** 2003. The Golgi apparatus at the cell centre. Curr. Opin. Cell Biol. **15:**60–66.
39. **Ríos, R. M., A. Sanchis, A. M. Tassin, C. Fedriani, and M. Bornens.** 2004. GMAP-210 recruits gamma tubulin complexes to cis-Golgi membranes and is required for Golgi ribbon formation. Cell **118:**323–335.
40. **Shen, K., Y. Wang, S. C. Brooks, A. Raz, and Y. A. Wang.** 2006. ATM is activated by mitotic stress and suppresses centrosome amplification in primary but not in tumor cells. J. Cell. Biochem. **99:**1267–1274.
41. **Shepard, J. L., J. F. Amatruda, D. Finkelstein, J. Ziai, K. R. Finley, H. M. Stern, K. Chiang, C. Hersey, B. Barut, J. L. Freeman, C. Lee, J. N. Glickman, J. L. Kutok, J. C. Aster, and L. I. Zon.** 2007. A mutation in separase causes genome instability and increased susceptibility to epithelial cancer. Genes Dev. **21:**55–59.
42. **Suizu, F., A. Ryo, G. Wulf, J. Lim, and K. P. Lu.** 2006. Pin1 regulates centrosome duplication, and its overexpression induces centrosome amplification, chromosome instability and oncogenesis. Mol. Cell. Biol. **26:**1463–1479.
43. **Szul, T., R. Grabski, S. Lyons, Y. Morohashi, S. Shestopal, M. Lowe, and E. Sztul.** 2007. Dissecting the role of the ARF guanine nucleotide exchange factor GBF1 in Golgi biogenesis and protein trafficking. J. Cell Sci. **120:**3929–3940.
44. **Tacconelli, A., A. R. Farina, L. Cappabianca, G. DeSantis, A. Tessitore, A. Vetuschi, R. Sferra, N. Rucci, B. Argenti, I. Screpanti, A. Gulino, and A. R. Mackay.** 2004. TrkA alternative splicing: a regulated tumor-promoting switch in human neuroblastoma. Cancer Cell **6:**347–360.
45. **Tacconelli, A., A. R. Farina, L. Cappabianca, G. Cea, A. Chioda, S. Panella, N. Rucci, A. Gulino, and A. R. Mackay.** 2006. Alternative TrkA splicing and cancer, p. 67–87. *In* J. P. Venebles et al. (ed.), Alternative splicing in cancer. Transworld Research Network, Kerala, India.
46. **Takahashi, T., and M. Shibuya.** 1997. The 230kDa mature form of KDR/Flk-1 (VEGF receptor-2) activates the PLC-gamma pathway and partially induces mitotic signals in NIH3T3 fibroblasts. Oncogene **14:**2079–2089.
47. **Tsou, M. F., and T. Stearns.** 2006. Mechanism limiting centrosome duplication to once per cell cycle. Nature **442:**947–951.
48. **Watson, F. L., M. A. Porcionatto, A. Bhattacharyya, C. D. Stiles, and R. A. Segal.** 1999. TrkA glycosylation regulates receptor localisation and activity. J. Neurobiol. **39:**323–336.
49. **Weber, R. G., J. M. Bridger, A. Benner, D. Weisenberger, V. Ehemann, G. Reifenberger, and P. Lichter.** 1998. Centrosome amplification as a possible mechanism for numerical chromosome aberrations in cerebral primitive neuroectodermal tumors with TP53 mutations. Cytogenet. Cell Genet. **83:**266–269.
50. **Wikstrand, C. J., R. E. McLendon, A. H. Friedman, and D. D. Bigner.** 1997. Cell surface localization and density of the tumor-associated variant of the epidermal growth factor, EGFRvIII. Cancer Res. **57:**4130–4140.
51. **Yoshida, H.** 2007. Unconventional splicing of XBP-1 mRNA in the unfolded protein response. Antioxid. Redox Signal. **9:**2323–2333.
52. **Yoshimura, S. I., N. Nakamura, F. A. Barr, Y. Misumi, Y. Ikehara, H. Ohuno, M. Sakaguchi, and K. Mihara.** 2001. Direct targeting of cis-Golgi matrix proteins to the Golgi apparatus. J. Cell Sci. **114:**4105–4115.
53. **Zyss, D., P. Montcourrier, B. Vidal, C. Anguille, F. Merezegue, A. Sahuquet, P. H. Mangeat, and P. J. Coopman.** 2005. The syk tyrosine kinase localises to the centrosome and negatively affects mitotic progression. Cancer Res. **65:**10872–10880.